A Peptide Derived from Sorting Nexin 1 Inhibits HPV16 Entry, Retrograde Trafficking, and L2 Membrane Spanning

Shuaizhi Li[1,2], Zachary L. Williamson[3], Matthew A. Christofferson[1,4], Advait Jeevanandam[1,5], Samuel K. Campos[1,6,7,8]

[1]Department of Immunobiology, University of Arizona, Tucson, AZ USA

[2]Current Address: Microbiologics, Inc. Saint Cloud, MN USA

[2]Biochemistry and Molecular & Cellular Biology Graduate Program, University of Arizona, Tucson, AZ USA

[4]Current Address: Department of Microbiology & Immunology, University of British Columbia, Vancouver, BC Canada

[5]Current Address: Department of Immunobiology, Yale University, New Haven, CT USA

[6]Department of Molecular & Cellular Biology, University of Arizona, Tucson, AZ USA

[7]Cancer Biology Graduate Interdisciplinary Program, University of Arizona, Tucson, AZ USA

[8]BIO5 Institute, University of Arizona, Tucson, AZ USA

Keywords: HPV16, minor capsid protein, L2, sorting nexin 1, SNX1, SNX-BAR, viral entry, retrograde trafficking, membrane spanning.

Abstract

High risk human papillomavirus (HPV) infection is responsible for 99% of cervical cancers and 5% of all human cancers worldwide. HPV infection requires the viral genome (vDNA) to gain access to nuclei of basal keratinocytes of epithelium. After virion endocytosis, the minor capsid protein L2 dictates the subcellular retrograde trafficking and nuclear localization of the vDNA during mitosis. Prior work identified a cell-permeable peptide termed SNX1.3, derived from the BAR domain of sorting nexin 1 (SNX1), that potently blocks the retrograde and nuclear trafficking of EGFR in triple negative breast cancer cells. Given the importance of EGFR and retrograde trafficking pathways in HPV16 infection, we set forth to study the effects of SNX1.3 within this context. SNX1.3 inhibited HPV16 infection by both delaying virion endocytosis, as well as potently blocking virion retrograde trafficking and Golgi localization. SNX1.3 had no effect on cell proliferation, nor did it affect post-Golgi trafficking of HPV16. Looking more directly at L2 function, SNX1.3 was found to impair membrane spanning of the minor capsid protein. Future work will focus on mechanistic studies of SNX1.3 inhibition, and the role of EGFR signaling and SNX1- mediated endosomal tubulation, cargo sorting, and retrograde trafficking in HPV infection.

Introduction

Human papillomaviruses (HPV) are among the most common sexually transmitted pathogens in the United States [1]. More than 220 HPV types have been identified and annotated, with reference genomes available in the PaVE database [2]. Within the genus *Alphapapillomavirus* there are 14 high-risk HPV types, of which HPV16 and HPV18 are the most prevalent [3]. High-risk HPV is responsible for 99% of cervical cancer and just under 5% of all human cancers worldwide [4,5]. HPV16 is alone responsible for roughly 50% of all cervical cancers in women and ~90% of the HPV-associated oropharyngeal cancers, mostly in men [4,6]. The nonavalent Gardasil-9 vaccine targets high-risk HPV16, HPV18, HPV31, HPV33, HPV45, HPV52, HPV58, and low risk HPV6 and HPV11, but it does not cover all the high-risk HPV types and the high cost prevents people in the low-income region to get access to the vaccine [4,7,8].

HPVs are small non-enveloped DNA viruses, with 72 disulfide-linked pentamers of major capsid protein L1 forming the icosahedral capsid [9]. Variable copies but less than 72 molecules (typically 20-40 molecules) of minor capsid protein L2 are incorporated within the viral particle, complexed with the ~8kb circular double-stranded viral DNA genome (vDNA) [10,11]. Although only a minor component of the virion, L2 plays an essential role in transporting the vDNA to the host cell nucleus during infection [12].

Successful infection requires HPV16 to gain access to the extracellular matrix (ECM)-rich basement membrane and basal keratinocytes of the differentiated epithelium [13]. At the cellular level, the initial attachment of the HPV16 to keratinocytes is via cell surface and ECM-localized heparin sulfate proteoglycans (HSPGs) [14,15]. Laminin-332 within the ECM has also been identified as an attachment molecule [16,17]. HSPG binding and extracellular furin- and kallikrein- dependent cleavage of the capsid proteins triggers conformational changes within the virion, allow it to engage a secondary entry complex [18–20]. Despite extensive study, the precise nature and composition of this entry complex remains obscure, but it likely contains growth factor receptor tyrosine kinases, integrins, tetraspanins, and annexin A2 [21–23]. Due in part to the time required for entry receptor complex assembly and capsid priming, HPV16 is asynchronously endocytosed by the host cell via macropinocytosis-like mechanisms, which are actin dependent but clathrin- and lipid raft-independent [18,24]. These uptake mechanisms are dependent upon signaling cascades initiated by receptor kinases such as EGFR and Abl2; bursts of EGFR signaling lead to activation of ERK and induction of pit formation while Abl2 kinase regulates maturation of endocytic pits during viral uptake [25]. Efficient trafficking of HPV16 also requires the inhibition of autophagy achieved via another EGFR signaling cascade that the virus uses to prime the cell for viral uptake [26,27]. Downstream of EGFR in this signaling cascade is the phosphoinositol 3-kinase/Akt/mTOR pathway, which can halt autophagy in the cell from activation by HPV16 [27]. EGFR has been known as one of the most important growth factor receptors in HPV entry and has had its role expanded and understood further in recent years [28].

Internalized virions traffic to the endosomal compartment, where the acidic environment in the endosome triggers the further disassembly of the viral capsid allowing for exposure of the L2/vDNA complex [29]. Meanwhile, the γ-secretase protease complex promotes membrane insertion of L2, to allow for spanning and protrusion of L2 through the vesicular membrane [30,31] via an N-terminal transmembrane domain [32]. Stable membrane spanning of L2 results in the cytosolic exposure of the C-terminal ~400 residues containing binding regions for cellular cargo sorting factors including SNX17, SNX27, and the heterotrimeric retromer complex [33–37]. Binding of these cytosolic factors to the cytosolic portion of transmembrane L2 facilitates efficient retrograde transport of the vesicle-bound vDNA to the *trans*-Golgi network [38], an obligate step of infection. Post-Golgi trafficking requires the onset of mitosis [39,40]. During this process, L2's chromosome-binding domain tethers the vDNA to host chromosomes to achieve nuclear delivery of L2/vDNA upon onset of the next G1 phase [41]. After mitosis, L2/vDNA recruits PML body components for efficient viral gene expression within the basal keratinocytes [42–44]. Once initial infection is established, episomal HPV16 vDNA will remain within these at a low copy number [13,45]. As the infected basal cells differentiate, expression of early viral genes, vDNA amplification, expression of late viral genes L1 and L2, and virion packaging and assembly will be coordinately achieved [46].

Retrograde trafficking of internalized L2/vDNA is a required step for HPV infection. The SNX-BAR subfamily of sorting nexins are key players in endocytosis, endosomal sorting, and vesicle trafficking. This family includes SNX1, SNX2, SNX4, SNX5, SNX6, SNX7, SNX8, SNX9, SNX18, SNX30, SNX32 and SNX33 [47]. A subgroup of the SNX-BAR family members, comprising SNX1, SNX2, SNX5, and SNX6 support sorting and retrograde transport of cargo from endosomes to the the Golgi [47,48]. SNX-BAR family proteins contain two major domains; the N-terminal PX domain that bind to specific phosphatidylinositol lipids in cellular membranes and a curved BAR domain that promotes protein-protein interactions and membrane remodeling [47,49]. Structurally, the curved BAR domains can form homo- and heterodimers with other SNX-BAR proteins to augment PX domain-dependent binding of the SNX-BAR protein to curved membranes, thereby supporting the tubulation of vesicles and the sorting of cargo into

115 these tubules for transport. Overexpression of SNX1 can result in BAR domain-
116 dependent bending and extensive tubulation of endosomal membranes. In certain
117 contexts, overexpression of SNX1 also promotes the interaction between the SNX1
118 BAR domain and EGFR, causing lysosomal degradation of the EGFR, a receptor that
119 has been shown important for HPV infection [50,51]. SNX2, which has a different
120 vesicular distribution pattern than SNX1, and less association with retromer compared
121 with SNX1, has also been shown to promote tubulation and regulate EGFR lysosomal
122 sorting [48,51,52]. Recent studies with cells genetically devoid of retromer components
123 Vps35 and Vps29 have revealed direct binding and sorting of specific cargo receptors
124 by SNX1/5 and SNX2/6 heterodimers, independently of the retromer complex [53–55].
125 These complexes, which facilitate tubular-based endosomal sorting of specific
126 transmembrane cargo proteins, have been termed “ESCPE-1” and are comprised of
127 SNX1/5 and SNX2/6 heterodimers [53,56].

128 Recently our colleagues [57] described a peptide therapeutic that kills epidermal growth
129 factor receptor (EGFR)-dependent triple negative breast cancer cells (TNBC) *in vitro*
130 and in mouse models. The peptide is named SNX1.3 and works by potently inhibiting
131 the retrograde nuclear trafficking of EGFR, a pathway crucial for TNBC survival [57].
132 The peptide is derived from residues 490-515 of the BAR domain of SNX1 (Fig 1A) and
133 is fused to a TAT-derived cell penetrating peptide called PTD4 [58] for efficient cellular
134 uptake. This alpha helical region of SNX1 lies at the interface of SNX1 BAR domain
135 homo- and heterodimers (Fig 1A) and is known to directly bind to the EGFR kinase
136 domain to alter signaling, trafficking and degradation [51,57]. Given that SNX1 is
137 involved in retrograde trafficking of EGFR and other receptor cargos, and that the
138 SNX1.3 peptide alters EGFR retrograde trafficking in TNBC cells [57], and the role of
139 EGFR in HPV16 infection, we sought to determine the effects of SNX1.3 on HPV
140 infection and trafficking.

141 Here, we observed strong and specific inhibition of HPV infection in multiple cell types
142 treated with SNX1.3 peptide. Unlike nuclear EGFR-dependent TNBC, SNX1.3 does not
143 affect keratinocyte viability or proliferation. Analysis of subcellular HPV trafficking
144 suggests SNX1.3 treatment delayed viral entry and caused a strong defect in viral

145 retrograde trafficking, attributable to the inhibition of L2 membrane spanning. These
146 data suggest a multi-step inhibition of the HPV infection by SNX1.3 peptide and
147 underscore the need for further mechanistic studies on interactions of the SNX1.3
148 peptide with cellular targets and studies of SNX-BAR proteins in both viral endocytosis
149 and retrograde sorting/trafficking.

150

151 **Materials and Methods.**

152 **Tissue culture.**

153 Immortalized human HaCaT keratinocytes [46] and murine K38 keratinocytes [59] were
154 cultured in high glucose DMEM media (GIBCO 11965-092) supplied with penicillin and
155 streptomycin (GIBCO 15140-122) and 10% fetal bovine serum (GIBCO A3160602).
156 HaCaT GFP-BAP cells, which stably express cytosolic GFP-BAP [40], were cultured in
157 the the parental HaCaT media supplemented with 0.2ug/ml of puromycin (Corning 61-
158 385-RA) to maintain GFP-BAP expression. 293TT cells were used for generating
159 HPV16 pseudoviruss were cultured in high-glucose DMEM media supplied with 10%
160 bovine growth serum (BGS, HyClone SH30541.03) and 165ug/ml hygromycin B
161 (Invitrogen 10687010) for selection. All cell lines were cultured in 5% CO_2 tissue culture
162 incubator at 37°C. Cells were passaged when their confluence was around 80-90%.
163 0.05% trypsin-EDTA (GIBCO® 25300-054) was used for trypsinizing the cells. For cell
164 counting 10μl 1:1 mixed suspended cells and trypan blue solution, 0.4% (w/v) in PBS
165 (Corning 25-900-CI) were applied to a hemocytometer for manual cell counting.

166

167 **Peptides.**

168 All peptides used in this project were generated by GenScript. Peptide stocks were
169 dissolved in ultrapure water at 1mM final concentration. The sequences are as follows;
170 PTD4: YARAAARQARA-acid, SNX1.3:
171 YARAAARQARAKNHVIKYLETLLYSQQQLAKYWEAFL-acid, SNX2.1:
172 YARAAARQARAKTVIIKYLESLVQTQQQLIKYWEAFL-acid.

173

174 **HPV16 PsVs production**

175 293TT cells were cultured in 10cm dishes. At the confluence around 50%, cells were
176 co-transfected with 15ug/plate of pGL3, a luciferase-expressing plasmid with SV40
177 origin of replication, and 15ug/plate of pXuLL-based plasmids (which express HPV16 L1
178 and L2) using $Ca_3(PO_4)_2$ transfection methods. The L2 packaged within these preps are
179 L2-3xFTHA, an HA-tagged form of L2 (L2-HA) previously shown to be infectious [60].
180 Plasmids were diluted into ultrapure water and 2M $CaCl_2$ solution, then mixed with
181 2xHBS (HEPES, buffered saline, 50mM HEPES, 280mM NaCl, 1.5mM Na_2PO_4)) to
182 generate DNA- $Ca_3(PO_4)_2$ crystal solution. Then it was incubated at room temperature
183 for 30m and added to the cells with gentle mixing. Fresh DMEM media containing 10%
184 BGS was changed the morning after transfection. 293TT cells were harvested at 48h
185 post-transfection. Cells were resuspended in PBS supplied with 9.5mM $MgCl_2$. and
186 lysed by 0.35% detergent Brij58. $(NH_4)_2SO_4$, pH=9.0 was added to 25mM to provide a
187 basic environment to promote L1 disulfide formation and viral capsid maturation [61].
188 Benzonase nuclease (Sigma E1014) was added to 0.3% final concentration and
189 Plasmid-Safe ATP-dependent DNase (Epicentre E3105K) was added to 20 U/ml final
190 concentration to digest any free unpackaged DNA. Lysates were incubated at 37°C, 5%
191 CO_2 in the tissue culture incubators for 20h, then ice chilled samples were
192 supplemented with 0.17 volume of 5M NaCl. Lysates were frozen and thawed at -80°C
193 and 37°C to further lyse the cell nuclei and release the viral particles. The samples were
194 centrifuged at 4°C at 10,000 x g for 10m. Pellets from this spin were resuspended in
195 viral storage buffer (VSB, 25mM HEPES with 500mM NaCl and 1mM MgCl2, pH=7.5),
196 and spun again. The two supernatants were pooled and loaded onto the top of the CsCl
197 gradient made by 4ml heavy (1.4g/ml, in VSB) CsCl and 4ml light (1.25g/ml, in VSB)
198 CsCl. Samples were centrifuged at 49,400 x g at 16°C for 18h by using Beckman SW41
199 Ti rotor/buckets. A visible, blueish-colored viral band appeared near the interface
200 between light and heavy CsCl after centrifugation. 18-gauge needles and 3ml syringes
201 were used for puncturing the side of the centrifuge tube to collect viral bands. 100 kDa
202 MWCO vivaspin concentrator units (Sartorius VS04T42) equilibrated with VSB were

203 used for washing and purifying the collected virus band. After the final wash, the virus
204 was concentrated to 100-200ul and transferred into siliconized tubes for storage at -
205 80°C. OD_{260} of DNA concentration of purified virus were measured by
206 spectrophotometer to calculate the concentration of physical viral particles. As HPV16
207 does not have a specific vDNA packaging signal, the content of the pGL3 in the purified
208 viruses was measured by SYBR green qPCR (Thermo Fisher K0252). The serial
209 dilution of the standard curve was used to determine the amount of pGL3 in virus
210 samples, the primers qLuc2-A (ACGATTTTGTGCCAGAGTCC), and qLuc2-B
211 (TATGAGGCAGAGCGACACC) were used for amplifying a portion of the firefly
212 luciferase gene on pGL3. Once the pGL3 concentration was measured, the
213 capsid/pGL3 ratios were determined. Physical titers (viral particles, or ng L1/unit
214 volume) were used for all experiments looking at intracellular levels of virus while pGL3
215 titers (pGL3 molecules/unit volume) were used for all infection experiments.

216

217 **Cell proliferation and cytotoxicity assays.**

218 For growth curve assay, 25,000 HaCaTs were seeded in 6 well plates along with 10μM
219 of peptide (PTD4 or SNX1.3) or water control, then after 24h, 48h, and 72h, cells from
220 each group were trypsinized and manually counted using a hemacytometer. For WST-1
221 assay, HaCaTs were plated at 6,000 cells/well in 96 well plates, in 100μl DMEM
222 supplied with 10% FBS. Once the cells were attached to the bottom, 10μM, 5μM,2.5μM
223 peptides were added to the cell cultures. Cells were incubated at 37°C and 5% CO_2 in
224 the presence of 2.5μM, 5μM, and 10μM peptides for 48h. Then, 10μl /well cell
225 proliferation reagent WST-1 (Roche 05015944001) was added, and cells were
226 incubated at 37°C, 5% CO_2 for another 4h. Plates were thoroughly shaken for 1m, and
227 the absorbance of formazan product was measured using a DTX800 Multimode plate
228 reader (Beckman Coulter) at 450nm. The cell-free media only group served as the
229 negative control for background subtraction.

230

231 **HPV16 PsV infection assay**

232 50,000 cells/well HaCaTs, HaCaT-GFP-BAP, mouse keratinocyte K38 or 80,000
233 cells/well 293TT cells were seeded in 24 well plates the day before infection. Cells were
234 infected with HPV16 at $2x10^8$ viral genome equivalents (pGL3 copies) per well under
235 the presence of 2.5μM, 5μM, and 10μM peptide. At 24h post-infection, cells were lysed
236 in 100μl reporter lysis buffer (RLB, Promega E397A). 100μl luciferase assay reagent
237 (Promega E1483) was added into 20μl cell lysate and luciferase activity was measured
238 using a DTX800 Multimode plate reader (Beckman Coulter). Western blots and GAPDH
239 immunostaining were performed by using the remaining lysate. GAPDH bands were
240 quantified by densitometry using ImageJ software [62] and used to normalize the
241 luciferase data.

242

243 **SDS-PAGE and western blotting**

244 For denaturing/reducing polyacrylamide gel electrophoresis (PAGE), samples were
245 lysed in RIPA lysis buffer (50mM Tris-HCl pH = 8.0, 150mM NaCl, 1% Triton X-100,
246 0.5% Na-deoxycholate, 0.5% SDS, supplemented with 1% PMSF (Sigma 78830) and
247 1% protease inhibitor cocktail (Sigma P8340), combined with 20% total volume of
248 denaturing/reducing SDS-PAGE buffer. Samples were then heated to 95°C for 5
249 minutes before separation on 10% or 12.5% polyacrylamide gels and run at 110V in
250 TGS running buffer (25mM Tris, 192mM glycine, 0.1% SDS, pH=8.6). Samples were
251 transferred onto nitrocellulose membranes under 300mA for 75m by using western
252 transfer buffer (25mM Tris, 192mM glycine) supplemented with 10% methanol.
253 Nitrocellulose membranes were then blocked with 5% non-fat milk in TBST (20mM Tris,
254 150mM NaCl, 0.1% Tween-20, pH = 7.5) at 4°C overnight. For the
255 denaturing/nonreducing PAGE, samples lysed by RIPA lysis buffer supplemented with
256 1% PMSF, 1% proteinase inhibitor, and 2mM N-ethylmaleimide (NEM, Sigma E1271)
257 were mixed with 20% total volume of denaturing /non-reducing SDS-PAGE buffer and
258 then incubated at room temperature for 10m before PAGE gel separation. RLB lysed
259 samples were added with 20% total volume of denaturing/reducing SDS-PAGE buffer
260 and incubated at 95°C for 5 mins before SDS-PAGE separation. For translocation
261 experiments, after the transfer step, Nitrocellulose membranes were blocked in

262 Odyssey Blocking Buffer PBS (LI-COR) at 4°C overnight. Antibodies used in western
263 blot are listed in table 2. Blots were imaged on the Licor Odyssey Infrared Imaging
264 System.

265

266 **Immunofluorescence staining and confocal microscopy.**

267 100,000 cells/well HaCaTs cells were plated on glass coverslips in 6 well plates. Cells
268 were infected with 1μg L1/ml of wt HPV16 PsVs with either 10μM PTD4 or SNX1.3
269 peptide. For some experiments, NH_4Cl was added to the infected cells to final
270 concentration of 20mM. For Golgi trafficking experiments, aphidicolin (Santa Cruz
271 38966-21-1) was added to a final concentration of 6μM. At 2h, 4h, 18h, or 24h post-
272 infection, cells were washed with high pH PBS (pH=10.6-10.8) for 2.5m to remove all
273 the surface-bound viruses, then fixed with 2% paraformaldehyde (pH = 7.2-7.4, Fisher
274 Scientific 30525-89-4) for 15m, permeabilized by 0.25% Triton X-100 (Fisher Scientific
275 9002-93-1) for 10m and blocked overnight by using blocking solution (PBS plus 4%
276 bovine serum albumin, fraction V, Fisher Scientific 9002-46-8, supplemented with 1%
277 goat serum). Cells were incubated with primary antibody at room temperature for 1h,
278 followed by 1h room temperature incubation of secondary antibody. All antibodies were
279 prepared in PBS containing 20% blocking solution. Prolong diamond anti-fade mounting
280 medium with DAPI (Life Technologies P36971) were used for mounting coverslips to the
281 glass slide. Confocal microscopy was performed by the Zeiss LSM880 system with
282 405nm, 488nm, and 543nm lasers. Samples were examined using a 63x objective, and
283 Z-stacks with a 0.35μm depth per plane were taken of each image. Images were
284 processed with Zen Blue software and ImageJ software. The Manders' overlap
285 coefficients were determined using the JACoP plugin on ImageJ under the thresholds
286 that were manually set below saturation [62]. The data were plotted with GraphPad
287 Prism v10 software. Antibodies used in immunofluorescence are listed in Table 1.

288

289 **Table 1. Antibodies used in this work.**

Antibody target and company	Species	Applications	Dilution	Working solution
GAPDH (Cell Signaling 2118S)	rabbit	WB	1:5,000	5% milk in TBST
HPV16 L1 Camvir-1 (Sc-47699)	mouse	WB	1:500	1% milk in TBST
GFP (Clontech 632377)	rabbit	WB	1:5,000	1% milk in TBST
NeutrAvidin Dylight 800-conjugate (Thermo 22853)	n/a	WB	1:10,000	LiCor blocking buffer
Vps35 (Abcam ab157220)	rabbit	WB	1:1000	1% milk in TBST
BAP31 (ThermoFisher MA3-002)	rat	WB	1:800	1% milk in TBST
HA (Roche 11867431001)	rat	IF/WB	1:1000	20% IF blocking buffer in PBS1% milk in TBST
P230 (BD Transduction Laboratories, #611280)	mouse	IF	1:400	20% IF blocking buffer in PBS
CD63 (Sigma SAB4700215)	mouse	IF	1:400	20% IF blocking buffer in PBS
HPV16 L1/L2 capsid (Gift from Dr. Michelle Ozbun)	rabbit	IF	1:1000	20% IF blocking buffer in PBS
TGN46 (Sigma-Aldrich T7576)	rabbit	IF	1:400	20% IF blocking buffer in PBS
LAMP1 (Cell Signaling 9091S)	rabbit	IF	1:400	20% IF blocking buffer in PBS

290 All IR680- and IR800-conjugated secondary antibodies (Fisher Scientific PI35518,
291 PISA535521, PI35568, PISA535571) were diluted 1:10,000 in 5% milk in 1X TBST.

292 All IF secondary antibodies including goat anti-mouse AlexaFluor-555 (Invitrogen
293 A21424), goat anti-rabbit AlexaFluor-488 (Invitrogen A11034), goat anti-rabbit

294 AlexaFluor-555 (Invitrogen A21429), goat anti-rat AlexaFluor-555 (Invitrogen A21434)
295 were prepared in 20% IF blocking buffer in PBS with 1:1,000 dilution.

296 **WB:** Western blot

297 **IF:** Immunofluorescence staining

298

299

300 **Image analysis for entry experiments.**

301 A protocol for measurement of total cell intensity using ImageJ [63] was used to quantify
302 the viral entry micrographs. Micrograph data were imported in ImageJ and the
303 selection tool was used to segment the border of single cells of the maximum intensity
304 composites for measurements. After the cells are segmented, the area, mean gray
305 value, and integrated density values were measured. A background region devoid of
306 cells was selected and analyzed from each field of view as well. Once all the
307 measurements were collected, the corrected total capsid channel fluorescence for each
308 segmented region was calculated as integrated density – (area of selected cell – mean
309 fluorescence of background readings). This process was manually done for all cells in
310 each field of view. The majority of the segmented regions contained a single cell, but
311 several contained doublets of cells that were difficult to individually segment. The
312 corrected total intensity of the capsid signal was then calculated and plotted between
313 PTD4 treated and SNX1.3 treated cells using GraphPad Prism v10.

314

315 **Viral binding and entry assays.**

316 Cells were chilled on ice for 20m before infecting with 1µg L1/ml of HPV16 under the
317 presence of 10µM of peptide in cold DMEM media supplemented with 10% FBS. Plates
318 were then stayed on the ice for 1h to allow surface binding of the viral particle. For the
319 binding sample, cells were first washed with cold PBS (pH = 7.4) to remove all unbound
320 viruses. Then the control groups were washed with cold high-pH PBS (pH = 10.75) to
321 remove the surface-bound virus. Samples were then collected for non-reducing SDS-
322 PAGE. For the entry sample, after 1h ice incubation viral pre-binding step, cells were
323 washed with cold PBS (pH = 7.4) to remove unbound viral particles, replaced with fresh
324 media, and incubated at 37°C, 5% CO_2. After 2h, cells were washed with high-pH PBS
325 to remove the surface-bound virus, replaced with fresh media, and returned to 37°C, 5%
326 CO_2. Samples were then collected at the indicated times and processed for non-

327 reducing SDS-PAGE. For some binding entry experiments, 20mM final concentration of
328 NH_4Cl were added to prevent viral degradation.

329

330 **L2-BirA membrane penetration assay.**

331 60,000 cells/well of HaCaT-GFP-BAP cells were plated in a 24-well plate. Cells were
332 infected with 150ng L1/well of HPV16 L2-BirA virus with 5μM or 10μM peptides. At 24h
333 post-infection, samples were processed for reducing SDS-PAGE followed by western
334 blot to detect total and biotinylated GFP.

335

336 **Aphidicolin release experiment.**

337 50,000 cells/well of HaCaTs were seeded in 24 well plates. Cells were then infected
338 with HPV16 at $2x10^8$ viral genome equivalents (pGL3 copies) per well under the
339 presence of 6μM aphidicolin. At 18h post-infection, cells were washed with high pH PBS
340 (pH=10.6-10.8) for 2.5 mins followed with two washes in regular PBS (pH=7.2-7.4) to
341 remove all the surface-bound virus and neutralize the pH. Then, fresh culture media
342 supplied with 6μM aphidicolin was added. After 8h incubation, the aphidicolin was
343 released by replacing with fresh media.

344

345 **Subcellular fractionation and alkaline membrane extraction.**

346 2 million HeLa-S3 cells were seeded in a 6cm dish. The following day cells are infected
347 with $1.25x10^5$ virions/cell at 37°C, 5% CO_2 for 24h in the presence of 10μM PTD4 or
348 SNX1.3 and 6μM aphidicolin to prevent viral trafficking beyond the Golgi. At the end of
349 the infection cells are rinsed with PBS and overlaid with 680μl swelling lysis buffer
350 (10mM HEPES pH=7.5, 1.5mM $MgCl_2$ hexahydrate, 10mM KCl, 0.5mM DTT, 1x
351 protease inhibitor cocktail (Sigma P8340), 1x PhosStop cocktail (Sigma) on ice for 30m.
352 Cells were collected by scraping and transferred to a 2ml Dounce homogenizer on ice.
353 Samples were homogenized with 30 full strokes of pestle B and transferred to microfuge

354 tubes. At this time, an 80μl aliquot of the sample corresponding to the "T total" fraction
355 was taken and combined with 20μl SDS-PAGE loading buffer and incubated at 90°C for
356 7m. The remaining sample was centrifuged at 10,000xg for 10 min at 4°C. Nuclear
357 pellets were discarded and 550μl the supernatant was transferred to 5x41mm ultra clear
358 centrifuge tubes (Beckman Coulter 344090). Samples were balanced and centrifuged at
359 42,000 rpm for 35m at 4°C in a SW55Ti rotor and buckets with tube adaptors (Beckman
360 REF: 356860). The supernatant was then concentrated to 80μl by spinning through
361 Amicon 3kDa MWCO concentrator units at 14,000xg for 15-30m at 4°C. These "S1
362 cytosol" fractions were then combined with 20μl SDS-PAGE loading buffer and heated
363 to 90°C for 7m. The pellets were gently rinsed (not resuspended) with 600μl HN buffer
364 (50mM HEPES pH=7.5, 150mM NaCl) and centrifuged again at 42,000 rpm for 35m at
365 4°C. The supernatant is discarded and the pellet from this step is rinsed and
366 resuspended in 50μl alkali buffer #1 (10mM Tris-HCl pH=7.5, 150mM NaCl, 2mM
367 MgCl2 hexahydrate, 5mM DTT) for 15m on ice, at which time 500μl alkali buffer #2 (100
368 mM Na_2CO_3 pH=11.7, freshly prepared) and samples are incubated for 30m on ice.
369 Samples were then spun at 42,000 rpm for 35m at 4°C to pellet the membranes.
370 Supernatants were collected and concentrated to 80μl by spinning through Amicon
371 3kDa MWCO concentrator units at 14,000xg for 15-30m at 4°C. These "S2 luminal and
372 peripheral proteins" were then mixed with 20μl SDS-PAGE loading buffer and heated to
373 90°C for 7m. Membrane pellets were rinsed with 600μl HN buffer and spun again at
374 42,000 rpm for 35m at 4°C. Supernatant was carefully removed and discarded, and
375 these final "P membrane" fractions were dissolved in 50μl SDS-PAGE loading buffer
376 and heated to 90°C for 7m. All fractions (T, S1, S2, P) were analyzed by SDS-PAGE
377 and western blotting for HA (L2), Vps35 (cytosolic retromer), and BAP31 (ER
378 membrane), as described above.

379

380 **Structural modeling, sequence alignment, and STRING analysis.**

381 The SNX1/SNX5 heterodimer (PDB 8AFZ) was rendered with PyMol [64], highlighting
382 the portion of SNX1 corresponding to the SNX1.3 peptide in red. The full structure is the

383 ESCPE-1 membrane coat [56], which contains a portion of the cation-independent
384 mannose phosphate receptor (CI-M6PR) in complex with the SNX1/SNX5 heterodimer.
385 The CI-M6PR density was removed for clarity. MacVector software was used for
386 sequence alignment of SNX1.3 and SNX2.1 peptides, using the ClustalW algorithm
387 [65]. STRING interaction network analysis was performed using STRING version 12.0
388 [66] webserver: [67]. “SNX1”, “SNX2”, and “EGFR” were used as the input queries.

389

390 **Results.**

391 **SNX1.3 blocks HPV16 infection in multiple cell lines.**

392 Infection experiments were performed using HPV16 pseudovirus encapsidating a firefly
393 luciferase reporter plasmid as described in *Materials and Methods*. SNX1.3 or control
394 PTD4 peptides were added at the time of infection and luciferase was assayed 24h post
395 infection. SNX1.3 treatment resulted in a dose-dependent inhibition of HPV16 infection
396 of HaCaT, 293TT, and murine K38 keratinocytes, whereas PTD4 control peptide had no
397 significant effects (Fig 1A, B). Calculated IC_{50} values were 3.8μM for 293TT, 2.6μM for
398 HaCaT, and 2.9μM for K38 keratinocytes (Fig 1C). Nearly two logs of inhibition were
399 observed at the 10μM dose in all three cell lines (Fig 1B, C). Mitosis is a requirement for
400 HPV16 infection [68], and 10μM SNX1.3 peptide was cytotoxic to triple negative breast
401 cancer cells [57], so it is important to determine if the peptide affects cell proliferation or
402 viability over these timeframes. 10μM PTD4 and SNX1.3 had only minor effects on cell
403 proliferation, extending the calculated doubling time of HaCaT cells from 24.7h hours to
404 25.8h and 28.2h respectively, as determined from exponential growth curve fitting of
405 total cell counts after 72h of continuous culture in the presence of peptides (Fig 1D).
406 The differences in cell proliferation were particularly minimal in the first 24h of growth,
407 the timeframe used for most experiments in this work. No significant differences in total
408 cell count were observed between the groups at any timepoint as determined by 2-way
409 ANOVA. SNX1.3 had no evidence of cytotoxicity compared to PTD4, as measured by
410 WST-1 assay (Fig 1E). Taken together, the data show that SNX1.3 effectively blocks

411 HPV16 pseudovirus infection in multiple cell types, and that this inhibition is not simply
412 due to general cytotoxicity or a block of mitosis.

413

414 **SNX1.3 peptide delays HPV16 entry.**

415 To understand SNX1.3 inhibition of HPV16 we began with binding and entry assays.
416 For binding assays HaCaT cells were chilled to 4°C and incubated with virus for 1h in
417 the presence of PTD4 or SNX1.3 peptides. Unbound virus was washed away with PBS
418 and some samples were treated with a high pH PBS buffer (pH = 10.75) to remove
419 bound virions [24]. Cells underwent additional PBS rinses and proteins were extracted
420 for non-reducing SDS-PAGE. Bound virions were detected by western blot for the
421 disulfide-bonded dimeric and trimeric forms of the major capsid protein L1. Figure 2A is
422 a representative blot, with quantified data including additional biological replicates
423 shown in Figure 2B. The data clearly shows that SNX1.3 has no significant impact on
424 virion binding and that high pH washing removes nearly all the surface bound virus,
425 which is important for the entry assays described below.

426 Next, we investigated the effects of SNX1.3 on viral endocytosis. In our initial
427 experiments, virions were prebound to HaCaT cells followed by a shift to 37°C for 3h, to
428 allow viral entry. After the 3h incubation, extracellular virus was cleared by high pH PBS
429 wash, and samples were either processed for non-reducing SDS-PAGE or given fresh
430 media and returned to 37°C for another 3h before processing for SDS-PAGE. Upon
431 return to 37°C, this “3h wave” of incoming virus will continue trafficking through the
432 endolysosomal pathway. As the virus traffics, L1 is cleaved by acid-dependent
433 endosomal proteases, resulting in the appearance of smaller degradation products
434 [19,69,70]. The data show lower levels of both intact L1 and degraded L1 upon
435 treatment with SNX1.3 compared to PTD4 (Supplemental Fig 1). Steady state levels of
436 intracellular L1 depend on both the rates of virion uptake and the rates of virion
437 degradation. Therefore, the observed differences in steady state L1 levels caused by
438 SNX1.3 could either be a result of slower uptake or accelerated degradation.

439 To differentiate between these two possibilities, and provide a means of obtaining more
440 quantitative data, we chose to eliminate the endo/lysosomal degradation of virions by
441 addition of NH_4Cl to the culture, which acts to buffer against endosomal acidification to
442 prevent activation of endosomal proteases [19,71]. To address the kinetics of viral
443 uptake, infections were done over a 6h time course in the presence of NH_4Cl. A high pH
444 wash was done at the end of each infection to measure only the intracellular virions at
445 the indicated times. The data show potent inhibition of HPV16 entry at 2h by SNX1.3
446 compared to PTD4 (Fig 3A, B). The lack of degraded L1 indicate show that the NH_4Cl
447 treatment was effective (Fig 3A) allowing us to measure cumulative entry. Over time,
448 the internalized virus increased steadily for both the PTD4 and SNX1.3 groups (Fig 3B).
449 Plotting the best fit linear regression of the data revealed nearly identical slopes (Fig
450 3C), indicating that SNX1.3 treatment substantially blunted early entry, but over time
451 virions enter at the same rate as the PTD4 group. The net result appears to be a delay
452 in viral uptake.

453 To confirm this phenotype, we performed immunofluorescence experiments, directly
454 visualizing intracellular virions by confocal microscopy. Cells were infected in the
455 presence of NH_4Cl and either PTD4 or SNX1.3 for 2h, 4h, or 18h prior to removal of
456 surface virus with high pH PBS, additional washing, fixation, and immunofluorescent
457 staining for the capsid and the endolysosomal markers CD63 or LAMP1. The
458 representative micrographs again show relatively poor uptake of virions in the presence
459 of SNX1.3 at early time points, but eventually the intracellular levels of capsid within
460 SNX1.3 treated cells become equivalent to those of the PTD4 treated group
461 (Supplemental Fig 2A). The micrographs also show that intracellular viruses are
462 colocalizing with endolysosomal markers in both groups, although the colocalization
463 with LAMP1 at 18h appears to be altered upon SNX1.3 treatment, perhaps suggestive
464 of altered trafficking. Quantification and normalization of the intracellular capsid signal to
465 cell number confirm the initial delay of viral uptake in the SNX1.3 treated groups
466 (Supplemental Fig 2B,C,D). Over time, the average intracellular levels of HPV16 virion
467 in the SNX1.3 treated group reach and even slightly surpass those of the PTD4 treated
468 group (Supplemental Fig 2D). The fact that SNX1.3 causes such a profound inhibition of
469 HPV16 infection suggests that SNX1.3 must be causing a secondary block to

470 subcellular viral trafficking, downstream of entry. Moving forward, we decided to focus
471 on this aspect of SNX1.3 activity.

472

473 **Late mitotic trafficking and limiting membrane penetration is blocked by SNX1.3.**

474 Successful HPV16 infection requires the delivery of the viral genome to the host cell
475 nucleus, a process dependent on mitosis [40,68,72]. During late mitotic trafficking,
476 vesicles containing the L2/vDNA complex traffic along microtubules, tethering on host
477 mitotic chromosomes via the central chromatin binding domain (residues 188-334)
478 within L2 [41]. The chromosome-bound vesicular L2/vDNA ends up in daughter cell
479 nuclei and the limiting vesicular membrane is quickly lost during this M/G1 transition
480 [39]. Loss of this vesicular membrane is important for the vDNA to access the cellular
481 transcriptional and replicative machinery necessary for successful infection. In prior
482 work we developed an assay for this late limiting membrane penetration, which we
483 termed “membrane translocation” at the time [40]. The assay is based on the
484 compartmentalization of the biotin-protein ligase BirA [73] away from its ectopically
485 expressed cytosolic substrate, GFP fused to a short biotin acceptor peptide [74](GFP-
486 BAP). Infection of GFP-BAP expressing HaCaT cells with HPV16 virions packaging an
487 L2-BirA fusion results in biotinylation of GFP-BAP only if L2-BirA can fully breach the
488 limiting membrane barrier during late mitotic trafficking. We first confirmed that SNX1.3
489 was inhibitory to L2-BirA virion infection of HaCaT-GFP-BAP cells (Fig 4A). Next, we
490 assayed the penetration of limiting membranes by detection of biotinylated GFP-BAP
491 using SDS-PAGE and western blot with IR800-conjugated fluorescent neutravidin. The
492 data show a strong GFP-biotin signal in PTD4 treated cells, but a strong reduction of
493 GFP-biotin in the presence of 5 μM and 10 μM SNX1.3 (Fig. 4B, C). Densitometry
494 shows a 75% and 95% decrease of L2-BirA membrane penetration with 5 μM and 10
495 μM SNX1.3 (Fig. 4C), suggesting that the very late stages of nuclear trafficking and
496 penetration of limiting membranes are blocked by SNX1.3.

497

498 **SNX1.3 blocks retrograde transport of HPV16 but does not affect post-Golgi**
499 **trafficking.**

500 As late trafficking and limiting membrane penetration are contingent on successful
501 retrograde transport of virions from endosomes to the Golgi [37,75], we next
502 investigated the effects of SNX1.3 on retrograde trafficking. For these experiments we
503 used virions packaged with HA-tagged L2 (L2-HA) to detect the presence of L2 in the
504 Golgi by immunofluorescence and confocal microscopy. We performed infections in the
505 presence of aphidicolin, a Polα/Polδ/Polε inhibitor that reversibly blocks cells in early S
506 phase [76]. Under these conditions HPV16 virions will retrograde traffic and accumulate
507 in the Golgi as the cells never reach G2/M, when Golgi egress and late nuclear
508 trafficking occur [77]. Cells were infected in the presence of aphidicolin and either PTD4
509 or SNX1.3 peptide for 24 hours prior to removal of surface virions with high pH PBS,
510 washing, fixation, and immunostaining for L2-HA, p230 Golgi marker, and DAPI. The
511 long 24h infection ensures that the SNX1.3-treated group has time to overcome the
512 early delay in endocytic uptake, as can be observed from the levels of L2-HA staining
513 (Fig 5A). The data clearly show strong accumulation of L2-HA in the p230-positive
514 trans-Golgi network in the presence of PTD4. In contrast, SNX1.3 treatment abolished
515 the overlap between L2-HA and p230, showing a clear defect in retrograde trafficking
516 (Fig 5A). Combined quantitative data of the Manders' colocalization coefficients from
517 three independent experiments show a statistically significant impairment of L2-
518 HA/p230 colocalization by the SNX1.3 peptide (Fig 5B).

519 We further tested whether SNX1.3 is still inhibitory after the virus has already reached
520 the *trans*-Golgi network. Aphidicolin is a reversible cell cycle inhibitor, once it is removed
521 by washout, viruses that are trapped in the *trans*-Golgi compartments will resume their
522 post-Golgi nuclear trafficking pathway once infected cells cycle into G2M [40,78]. The
523 experimental setup is shown in the Fig 6A. HaCaT cells were infected with HPV16 in the
524 presence of 6μM aphidicolin for 18h prior to high pH PBS removal of surface bound
525 virus. Since viral uptake is not synchronized, cells were further incubated in media with
526 6μM aphidicolin for another 8h to allow the intracellular virions additional time to reach
527 *trans*-Golgi network. At 26h post infecton, cells were released from aphidicolin by

528 washing and replacing with media containing either PTD4 or SNX1.3 peptide for an
529 additional 24h prior to luciferase assay. We did not observe any significant inhibition of
530 infection by SNX1.3 in this assay (Fig. 6B). These data show that HPV16 fails to
531 undergo efficient retrograde trafficking in the presence of SNX1.3, but once the virus
532 has reached the Golgi, SNX1.3 treatment is no longer inhibitory.

533

534 **SNX1.3 inhibits L2 membrane spanning.**

535 The minor capsid protein L2 is required for the retrograde transport of the vDNA. After
536 endocytic uptake, L2 is inserted into the local endosomal membrane to adopt a type-I
537 transmembrane protein topology [33], spanning via its single N-terminal transmembrane
538 domain [32]. Precise mechanisms of L2 spanning remain obscure, but the process is
539 dependent on numerous cellular factors including furin, p120 catenin, γ-secretase, and
540 endosomal acidification, in addition to a positively charged cell penetrating peptide near
541 the C-terminus of L2 [30,31,79]. Membrane spanning in this manner allows ~400 C-
542 terminal residues downstream of the transmembrane domain to protrude into the
543 cytosol to recruit retromer and other sorting factors necessary for efficient retrograde
544 trafficking to the Golgi [34,35,37]. We therefore wanted to determine if the block in
545 retrograde trafficking by SNX1.3 was due to a defect in membrane spanning.

546 To measure spanning we adopted an alkali membrane extraction protocol recently
547 described by the Tsai Lab [31]. This stringent subcellular fractionation protocol relies on
548 sequential high-speed centrifugations and a harsh alkali wash step to isolate only *bona*
549 *fide* integral transmembrane proteins in the final membrane pellet. HeLa-S3 cells were
550 infected in the presence of either PTD4 or SNX1.3 for 24h. Aphidicolin was included in
551 the media to prevent virion traffic beyond the Golgi in this long infection. Cells were
552 gently lysed and fractionated as described in *materials and methods*. We collected four
553 fractions: T; total cell fraction, S1; cytosolic protein, S2; luminal organelle and peripheral
554 membrane proteins, and P; integral membrane proteins. Samples were analyzed by
555 SDS-PAGE and immunoblotting for L2-HA, the cytosolic marker Vps35, and the ER
556 transmembrane protein BAP31. Results show a clear reduction in L2 membrane
557 spanning in the presence of SNX1.3 (Fig 7A). Results from three independent

558 experiments were quantified by densitometry, normalizing the membrane-spanning L2
559 signal in the P fractions to both the BAP31 membrane marker and the total L2 signal in
560 the T fraction, revealing a strong and statistically significant defect in membrane
561 spanning upon addition of SNX1.3 peptide (Fig 7B). These data suggest that SNX1.3
562 blocks retrograde trafficking of virus by somehow preventing the membrane spanning
563 ability of L2.

564

565 **Discussion.**

566 Previously, the SNX1.3 peptide was found to inhibit EGFR retrograde nuclear trafficking
567 in TNBC cells, causing cell death [57]. Here, we investigate the inhibition of HPV16
568 pseudovirus infection by the SNX1.3 peptide in human HaCaT keratinocytes, 293TT
569 cells, and mouse K38 keratinocytes. We found the peptide did not impair cell viability or
570 proliferation of these cells, in contrast to the nuclear EGFR-dependent TNBC. SNX1.3
571 impaired HPV16 infection with low micromolar IC_{50} values, causing a delayed uptake
572 phenotype in HaCaT cells. Given time, HPV16 virions eventually overcome this entry
573 delay but SNX1.3 peptide treatment imposed a strong block to late nuclear trafficking
574 and retrograde Golgi trafficking of L2/vDNA. Once virus reached the Golgi, infection was
575 resistant to SNX1.3 treatment, demonstrating that the block in trafficking was pre-Golgi.
576 Alkaline membrane fractionation experiments revealed that the block in retrograde
577 trafficking by SNX1.3 was due to a defect in L2 membrane spanning, a necessary step
578 for viral retrograde trafficking. We have not yet tested whether the SNX1.3 peptide is
579 inhibitory to diverse HPV types, nor have we tested if the SNX1.3 peptide directly binds
580 to L1 or L2 proteins of the HPV capsid.

581 Clearly more work is needed to determine if the delayed entry phenotype is due to
582 EGFR-dependent mechanisms but SNX1 overexpression can alter EGFR signaling,
583 endocytosis, retrograde trafficking, recycling, and degradation [51,80–82]. The effects of
584 the SNX1.3 peptide on endogenous SNX1 and SNX-BAR function remain to be
585 determined but it could be envisioned that the peptide may act as a dominant negative
586 form of SNX1 in some contexts and/or excess peptide could mimic SNX1
587 overexpression in other contexts. These details remain to be determined experimentally

588 but it is worth noting that the peptide is derived from a region of the SNX1 BAR homo-
589 /heterodimerization interface and may outcompete these natural interactions (Fig 1A),
590 and many networks and interactions with cellular partners could be perturbed by the
591 introduction of such a peptide into the system (Supplemental Fig 3). The patterns of
592 endolysosomal markers CD63 and LAMP1 appeared to be slightly altered by SNX1.3
593 treatment (supplemental Fig 2), suggesting that SNX1.3 treatment may result in a global
594 (but subtle) perturbation of vesicular trafficking and/or altered localization of cellular
595 proteins which may affect HPV16 trafficking.

596 It is also notable that this region of SNX1 has a high degree of amino acid identity with
597 the corresponding region of SNX2 (Fig 8A) and it is reasonable to posit that SNX1.3
598 may interfere with SNX2-partner interactions via this conserved region. Indeed, we
599 found the analogous SNX2-derived peptide SNX2.1 displayed strong inhibition of
600 HPV16 infection (Fig 8B) although further work is needed to validate the same delayed
601 entry phenotype and retrograde trafficking blocks. SNX2 was recently described to
602 contribute to HPV16 endocytosis via a macropinocytosis-like EGFR/Abl2/WASH/actin-
603 dependent mechanism [83]. In that work SNX2 was found to be present at HPV16 entry
604 sites and depletion of SNX2 by siRNA was shown to inhibit viral uptake [83].

605 The observed entry defect upon SNX1.3 treatment was merely a delay, with virions
606 eventually overcoming this block. The strong block imposed by SNX1.3 was instead due
607 to inhibition of retrograde trafficking. After entry, L2 adopts a membrane spanning
608 conformation to gain access to cytosolic retromer and other sorting factors needed for
609 efficient transport to the Golgi [28]. As SNX1/2/5/6 heterodimers can partner with
610 retromer for retrograde transport of transmembrane cargo [47,52,84,85] we expected to
611 observe normal L2 membrane spanning with a defect in transport upon SNX1.3
612 treatment. Rather, we observed a strong defect in L2 membrane spanning, suggesting
613 involvement of SNX-BAR proteins or cellular partners in this process. The retromer
614 complex was recently shown to play a role in stable membrane insertion of L2—early
615 membrane spanning was stabilized by the binding of cytosolic retromer to its binding
616 sites near the C-terminus of L2 [86]. Further work is needed to determine if SNX1 and

617 related SNX-BAR proteins augment this retromer-dependent function to support L2
618 membrane insertion.

619 Alternatively, it may be that membrane tubulation and curvature are involved. HPV16
620 and diverse HPV types induces endosomal tubulation during entry, in an EGFR and
621 VAP-dependent manner [87,88]. SNX2 is a known partner of VAPB and SNX2 partners
622 with SNX1 to promote endosomal tubulation and sorting of cargo into autophagosomes
623 upon nutrient starvation [89]. Tubulation of endosomes may generate positive
624 membrane curvature on the lumenal face of endosomes, to aid in the membrane
625 penetration of the C-terminal L2 cell penetrating peptide [79] and/or transmembrane
626 domain [32]. Membrane curvature has been demonstrated to augment the activity of
627 octaarginine cell penetrating peptide [90] and local membrane environment may greatly
628 affect the ability of proteins like L2 to insert and span across membranes [91]. Further
629 work is necessary to delineate the exact mechanisms behind the SNX1.3-imposed
630 blocks we observe in this study, but this work lays the groundwork for some interesting
631 testable hypotheses regarding potential roles of SNX-BAR proteins and their cellular
632 partners in HPV16 infection.

633

634 **Acknowledgements.**

635 This work was supported by grants 1R01GM136853-01 and 1R35GM152143-01 from
636 the National Institute of General Medical Sciences. We are grateful to Dr. Joyce
637 Schroeder and Dr. Ben Atwell for the PTD4, SNX1.3, and SNX2.1 peptides and fruitful
638 scientific discussions. We thank Dr. Michelle Ozbun for the anti-HPV16 polyclonal
639 antibody. We thank Dr. Koenraad van Doorslaer and members of the Van Doorslaer
640 Lab and the Campos Lab for valuable scientific discussions.

641

642 **Author Contributions**

SKC and SL designed and conceived the experiments. SL, ZLW, MAC, AJ, and SKC performed the experiments, analyzed the data, and prepared figures. SKC and SL wrote the paper.

651 **Figure Legends**

652 **Fig 1. Inhibition of HPV16 infection by SNX1.3 peptide. (A)** Sequences of the control
653 PTD4 cell penetrating peptide and the SNX1.3 peptide. SNX1.3 is derived from residues
654 490-515 of the SNX1 BAR domain. This portion is highlighted (red) within the context of
655 the SNX1/SNX5 heterodimer (PDB 8AFZ), at the interface of the BAR domains. **(B)**
656 Infectivity of firefly luciferase expressing HPV16 in multiple cell types in the presence of
657 10 μM PTD4 or SNX1.3 peptide, compared to H_2O vehicle control. **(C)** Titration of
658 peptides showing dose-dependent inhibition of HPV16 infection in multiple cell types.
659 For **(B, C)**, the graphs show mean infectivity ± SEM. For **(C)** all groups were statistically
660 significant $p<0.05$ except for PTD4 vs SNX1.3 in 293TT. **(D)** Growth curves of HaCaT
661 cells ± 10 μM PTD4 or SNX1.3 peptide, compared to H_2O vehicle control. No statistical
662 significance was observed by between groups at any particular timepoint. **(E)** WST-1
663 assay for HaCaT cell viability ± PTD4 or SNX1.3 peptide. Assay performed 48h post
664 seeding with peptides. Graph shows mean percent 450nm absorbance ± SEM. All
665 statistics were determined by 2-way ANOVA with Tukey's multiple comparison. *$p<0.05$,
666 ****$p<0.0001$.

667

668 **Fig 2. HPV16 binding assay. (A)** HPV16 was bound to HaCaT cells ± 10uM PTD4 or
669 SNX1.3 for 1h at 4°C. Cells were then washed with regular PBS to remove unbound
670 virus in the media or washed with high pH PBS to remove the surface-bound virus as
671 well. Cell surface-bound L1 dimers and trimers were detected by non-reducing SDS-
672 PAGE and western blot, as described in *Materials and Methods*. A representative L1
673 blot is shown, along with GAPDH loading control. **(B)** Densitometric quantification of
674 intact HMW L1 band intensities was performed by ImageJ. Graphs show mean relative
675 L1 band intensities at given times, n = 3 independent biological replicates, relative to the
676 PTD4 treated groups. Statistics were determined using 2-way ANOVA with Šídák's
677 multiple comparison test. ****$p<0.0001$.

678

679 **Supplemental Fig1. HPV16 entry assay, 3h wave.** HPV16 was bound to HaCaT cells
680 ± 10μM PTD4 or SNX1.3 for 1h at 4°C. Cells were then incubated for at 37°C for 3h to
681 allow viral entry. At this time cell surface virus was removed by high pH PBS wash in all
682 the groups. Media containing ± 10μM PTD4 or SNX1.3 peptides was replaced, and cells
683 were incubated at 37°C for another 3hrs (6h time group) to allow the existing
684 intracellular virus to traffic through the endocytic pathway. Samples were processed as
685 described above and collected at 3h or 6h post-entry. Cell lysates were processed for
686 non-reducing SDS-PAGE and western blot to detect intact and degraded forms of L1.
687 Non-specific bands (n.s.) is a cellular protein that cross-reacts with the L1 antibody, and
688 serves as an internal loading control.

689

690 **Fig 3. SNX1.3 delays HPV16 entry. (A)** HPV16 was bound to HaCaT cells ± 10μM
691 PTD4 or SNX1.3 and 20 mM NH_4Cl for 1h at 4°C. Cells were then incubated at 37°C for
692 2h, 4h, or 6h at which time cell surface virus was removed by high pH PBS wash at the
693 time of sample collection. Cell lysates were processed for non-reducing SDS-PAGE and
694 western blot to detect intact and degraded forms of L1. Non-specific bands (n.s). is a
695 cellular protein that cross-reacts with the L1 antibody and serves as an internal loading
696 control. In this manner cumulative viral uptake can be visualized as more and more
697 virions enter the cells over the timecourse and degradation is blocked by NH_4Cl.
698 Representative blot is shown. **(B)** Densitometric quantification of intact HMW L1 band
699 intensities was performed by ImageJ. Graphs show mean relative L1 band intensities at
700 given times (±SEM, n = 3 independent biological repeats) relative to the PTD4 treated
701 group at 6h time point. Simple linear regression was used to plot the lines. Statistics
702 were determined using multiple unpaired t-tests. *$p<0.05$.

703

704 **Supplemental Fig2. Immunofluorescence entry assay. (A)** HaCaT cells plated on
705 glass coverslips were infected with HPV16 bearing L2-3xFTHA ± 10μM PTD4 or
706 SNX1.3 and 20 mM NH_4Cl for 2h, 4h, or 18h followed by high pH PBS wash to remove
707 the surface-bound virus. Cells were then processed for IF and capsid, endolysosomal

708 markers, and nuclei were stained and mean fluorescence intensity of intracellular capsid
709 signal was quantified as described in *Materials and Methods*. **(B, C, D)** Mean and all
710 individual data points are plotted from n=3 biological replicates. Statistics were
711 determined using multiple unpaired t-tests. ***p<0.005, ****p<0.0001. Scale bars, 20
712 μm.

713

714 **Fig 4. Late membrane penetration is blocked by SNX1.3. (A)** Infectivity of luciferase-
715 expressing HPV16 packaged with L2-BirA with 10μM PTD4, SNX1.3, or H2O (solvent
716 vehicle control) in the HaCaT-GFP-BAP cell line. **(B)** L2-BirA membrane translocation
717 assay. HaCaT-GFP-BAP cells were infected with HPV16 bearing L2-BirA with 10μM
718 PTD4 or SNX1.3 peptides. Cells were processed for SDS-PAGE and western blotting at
719 24h post-infection, blotting for biotin-GFP and total GFP. Biotinylation of GFP can only
720 occur if L2-BirA penetrates the limiting vesicular membrane during late mitotic trafficking
721 of virions **(C)** Quantification of the membrane translocation assay. Band intensities were
722 measured by densitometry using ImageJ. The 10μM PTD4 treated cells were set to
723 100%, The graph represents the mean percent biotin-GFP normalized with total GFP
724 ±SEM, n = 4 independent biological replicates. Statistics were determined using 1-way
725 ANOVA with Šídák's multiple comparison test. ****p<0.0001.

726

727 **Fig 5. SNX1.3 blocks HPV16 retrograde trafficking to the Golgi. (A)** HaCaT cells
728 were infected at 37°C with HPV16 bearing L2-HA tag for 24h together with 6 μM
729 aphidicolin and either 10μM PTD4 or SNX1.3 peptide at 37°C for 24hrs followed by a
730 high pH wash to remove the surface-bound virus before fixation and processing for IF
731 staining as described in *Materials and Methods*. Cells were stained with mouse anti-
732 p230 with AlexaFluor-488 conjugated anti-mouse secondary (green), and rat anti-HA
733 with AlexaFluor-555 conjugated anti-rat secondary (red). The cell nucleus was stained
734 with DAPI (blue). Scale bars, 20 μm (**B)** Colocalization analysis using the JACoP plugin
735 of ImageJ. Manders' overlap coefficients were measured between L2-HA:p230 for
736 multiple Z-stacks, each containing multiple cells/field, from 3 independent experiments.

737 The mean Manders' coefficient of each biological replicate ±SEM are shown in black
738 bars, dots are the mean Manders' coefficient for each biological replicate, each
739 determined from numerous technical replicate measurements. Statistics were
740 determined using unpaired t-tests. **p<0.01.

741

742 **Fig 6. SNX1.3 has no effect on post-Golgi trafficking. (A)** Schematic of aphidicolin
743 release infection experiment. HaCaTs were infected with HPV16 at 37°C in the
744 presence of 6μM aphidicolin for 18h followed with high pH PBS (pH=10.6-10.8) wash to
745 remove all the surface-bound virus. Fresh culture media supplemented with 6μM
746 aphidicolin was then added for another 8h incubation at 37°C. This allows for
747 intracellular viruses to retrograde traffic to the Golgi. Aphidicolin was then released by
748 replacing media with containing either 10 μM PTD4 or SNX1.3 peptide for another 24h
749 at 37°C to allow nuclear trafficking of virus and the expression of luciferase. **(B)**
750 Infectivity of luciferase-expressing HPV16 in the aphidicolin release experiment,
751 normalized to PTD4 treatment. Mean infectivity ±SEM are plotted from n=3 biological
752 replicates. Statistics were determined with a two-sample unpaired t-test.

753

754 **Fig 7. SNX1.3 blocks L2 membrane spanning. (A)** Subcellular fractionation and alkali
755 membrane extraction blot of membrane spanning L2. HeLa-S3 cells were infected with
756 HPV16 bearing L2-HA in the presence of 10μM PTD4 or SNX1.3 peptide and 6μM
757 aphidicolin as described in *Materials and Methods*. After 24h cells were processed for
758 fractionation and alkaline membrane extraction. Total (T), S1 (supernatant 1; cytosolic
759 proteins), S2 (supernatant 2; organelle lumenal and peripheral membrane proteins), and
760 P (final pellet; integral membrane proteins) were collected as described and analyzed
761 by SDS-PAGE and western blotting for BAP31 (integral ER membrane protein), Vps35
762 (soluble cytosolic protein), and L2-HA. Representative blot is shown. **(B)** Densitometric
763 quantification of L2 membrane spanning. L2 densities within the membrane and total
764 fractions were first normalized to their corresponding BAP31 densities to account for
765 sample loss during fractionation and potential differences in gel loading. Then the

766 membrane L2 density was divided by the total L2 density, with the PTD4 membrane L2
767 values being adjusted to 100. Mean relative L2 spanning values ±SEM are plotted from
768 n=3 biological replicates. Statistics were determined with a two-tailed unpaired t-test.
769 ***p<.005.

770

771 **Fig 8. Inhibition of HPV16 infection by SNX2.1 peptide. (A)** Sequence alignment of
772 the SNX1.3 and SNX2.1 peptides. **(B)** Infectivity of HPV16 in HaCaT cells in the
773 presence of 10 μM PTD4, SNX1.3, or SNX2.1 peptides. Graphs show mean infectivity ±
774 SEM. N=3 biological replicates. Statistics were determined by 1-way ANOVA with
775 Dunnett's multiple comparison, ****p<0.0001.

776

777 **Supplemental Fig 3. STRING network analysis of SNX1/SNX2/EGFR. (A)** STRING
778 version 12.0 was used to analyze the interaction network of SNX1, SNX2, and EGFR.
779 Nodes include other SNX-BAR family members, other SNX proteins, retromer
780 components, WASH components, and the Rab GTPase activating protein TBC1D5,
781 many of which are cellular proteins known to be important for HPV16 trafficking and
782 infection. **(B)** Screenshot of the network analysis legend, explaining the nodes, edges,
783 input, and predicted partners.

784

785

786

787

788

789

790

791

792

793 **References**

794 1. **HPV Facts & Brochures | CDC**. 2022,

795 2. Van Doorslaer K, Li Z, Xirasagar S, Maes P, Kaminsky D, Liou D, Sun Q, Kaur R,
796 Huyen Y, McBride AA: **The Papillomavirus Episteme: a major update to the**
797 **papillomavirus sequence database**. *Nucleic Acids Res* 2017, **45**:D499–D506.

798 3. **HPV and Cancer - NCI**. 2019,

799 4. Forman D, de Martel C, Lacey CJ, Soerjomataram I, Lortet-Tieulent J, Bruni L,
800 Vignat J, Ferlay J, Bray F, Plummer M, et al.: **Global burden of human**
801 **papillomavirus and related diseases**. *Vaccine* 2012, **30 Suppl 5**:F12-23.

802 5. Schiffman M, Doorbar J, Wentzensen N, de Sanjosé S, Fakhry C, Monk BJ, Stanley
803 MA, Franceschi S: **Carcinogenic human papillomavirus infection**. *Nat Rev Dis*
804 *Primers* 2016, **2**:16086.

805 6. Lechner M, Liu J, Masterson L, Fenton TR: **HPV-associated oropharyngeal**
806 **cancer: epidemiology, molecular biology and clinical management**. *Nat Rev*
807 *Clin Oncol* 2022, **19**:306–327.

808 7. Brotherton JML, Ogilvie GS: **Current status of human papillomavirus**
809 **vaccination**. *Curr Opin Oncol* 2015, **27**:399–404.

810 8. Zhai L, Tumban E: **Gardasil-9: A global survey of projected efficacy**. *Antiviral*
811 *Res* 2016, **130**:101–109.

812 9. Buck CB, Day PM, Trus BL: **The papillomavirus major capsid protein L1**.
813 *Virology* 2013, **445**:169–174.

814 10. Buck CB, Cheng N, Thompson CD, Lowy DR, Steven AC, Schiller JT, Trus BL:
815 **Arrangement of L2 within the papillomavirus capsid**. *J Virol* 2008, **82**:5190–
816 5197.

817 11. Wang JW, Roden RBS: **L2, the minor capsid protein of papillomavirus**.
818 *Virology* 2013, **445**:175–186.

819 12. Campos SK: **Subcellular Trafficking of the Papillomavirus Genome during**
820 **Initial Infection: The Remarkable Abilities of Minor Capsid Protein L2**. *Viruses*
821 2017, **9**:E370.

822 13. Doorbar J, Quint W, Banks L, Bravo IG, Stoler M, Broker TR, Stanley MA: **The**
823 **biology and life-cycle of human papillomaviruses**. *Vaccine* 2012, **30 Suppl**
824 **5**:F55-70.

825 14. Kines RC, Thompson CD, Lowy DR, Schiller JT, Day PM: **The initial steps**
826 **leading to papillomavirus infection occur on the basement membrane prior to**
827 **cell surface binding**. *Proc Natl Acad Sci U S A* 2009, **106**:20458–20463.

828 15. Shafti-Keramat S, Handisurya A, Kriehuber E, Meneguzzi G, Slupetzky K,
829 Kirnbauer R: **Different heparan sulfate proteoglycans serve as cellular**
830 **receptors for human papillomaviruses**. *J Virol* 2003, **77**:13125–13135.

831 16. Culp TD, Budgeon LR, Marinkovich MP, Meneguzzi G, Christensen ND:
832 **Keratinocyte-secreted laminin 5 can function as a transient receptor for**
833 **human papillomaviruses by binding virions and transferring them to adjacent**
834 **cells**. *J Virol* 2006, **80**:8940–8950.

835 17. Brendle SA, Christensen ND: **HPV Binding Assay to Laminin-332/Integrin**
836 **α6β4 on Human Keratinocytes**. In *Cervical Cancer: Methods and Protocols*. Edited
837 by Keppler D, Lin AW. Springer; 2015:53–66.

838 18. Becker M, Greune L, Schmidt MA, Schelhaas M: **Extracellular Conformational**
839 **Changes in the Capsid of Human Papillomaviruses Contribute to**
840 **Asynchronous Uptake into Host Cells**. *J Virol* 2018, **92**.

841 19. Cerqueira C, Samperio Ventayol P, Vogeley C, Schelhaas M: **Kallikrein-8**
842 **Proteolytically Processes Human Papillomaviruses in the Extracellular Space**
843 **To Facilitate Entry into Host Cells**. *J Virol* 2015, **89**:7038–7052.

844 20. Richards RM, Lowy DR, Schiller JT, Day PM: **Cleavage of the papillomavirus**
845 **minor capsid protein, L2, at a furin consensus site is necessary for infection**.
846 *Proc Natl Acad Sci U S A* 2006, **103**:1522–1527.

847 21. Mikuličić S, Florin L: **The endocytic trafficking pathway of oncogenic**
848 **papillomaviruses**. *Papillomavirus Res* 2019, **7**:135–137.

849 22. Mikuličić S, Strunk J, Florin L: **HPV16 Entry into Epithelial Cells: Running a**
850 **Gauntlet**. *Viruses* 2021, **13**:2460.

851 23. Ozbun MA: **Extracellular events impacting human papillomavirus infections:**
852 **Epithelial wounding to cell signaling involved in virus entry**. *Papillomavirus Res*
853 2019, **7**:188–192.

854 24. Schelhaas M, Shah B, Holzer M, Blattmann P, Kühling L, Day PM, Schiller JT,
855 Helenius A: **Entry of human papillomavirus type 16 by actin-dependent,**
856 **clathrin- and lipid raft-independent endocytosis**. *PLoS Pathog* 2012,
857 **8**:e1002657.

858 25. Bannach C, Brinkert P, Kühling L, Greune L, Schmidt MA, Schelhaas M:
859 **Epidermal Growth Factor Receptor and Abl2 Kinase Regulate Distinct Steps of**
860 **Human Papillomavirus 16 Endocytosis**. *J Virol* 2020, **94**.

861 26. Griffin LM, Cicchini L, Pyeon D: **Human papillomavirus infection is inhibited**
862 **by host autophagy in primary human keratinocytes**. *Virology* 2013, **437**:12–19.

863 27. Surviladze Z, Sterk RT, DeHaro SA, Ozbun MA: **Cellular entry of human**
864 **papillomavirus type 16 involves activation of the phosphatidylinositol 3-**
865 **kinase/Akt/mTOR pathway and inhibition of autophagy**. *J Virol* 2013, **87**:2508–
866 2517.

867 28. Ozbun MA, Campos SK: **The long and winding road: human papillomavirus**
868 **entry and subcellular trafficking**. *Curr Opin Virol* 2021, **50**:76–86.

869 29. Smith JL, Campos SK, Wandinger-Ness A, Ozbun MA: **Caveolin-1-dependent**
870 **infectious entry of human papillomavirus type 31 in human keratinocytes**
871 **proceeds to the endosomal pathway for pH-dependent uncoating**. *J Virol* 2008,
872 **82**:9505–9512.

873 30. Harwood MC, Dupzyk AJ, Inoue T, DiMaio D, Tsai B: **p120 catenin recruits**
874 **HPV to γ-secretase to promote virus infection**. *PLoS Pathog* 2020, **16**:e1008946.

875 31. Inoue T, Zhang P, Zhang W, Goodner-Bingham K, Dupzyk A, DiMaio D, Tsai B:
876 **γ-Secretase promotes membrane insertion of the human papillomavirus L2**
877 **capsid protein during virus infection**. *J Cell Biol* 2018, **217**:3545–3559.

878 32. Bronnimann MP, Chapman JA, Park CK, Campos SK: **A transmembrane**
879 **domain and GxxxG motifs within L2 are essential for papillomavirus infection**.
880 *J Virol* 2013, **87**:464–473.

881 33. DiGiuseppe S, Keiffer TR, Bienkowska-Haba M, Luszczek W, Guion LGM, Müller
882 M, Sapp M: **Topography of the Human Papillomavirus Minor Capsid Protein L2**
883 **during Vesicular Trafficking of Infectious Entry**. *J Virol* 2015, **89**:10442–10452.

884 34. Pim D, Broniarczyk J, Bergant M, Playford MP, Banks L: **A Novel PDZ Domain**
885 **Interaction Mediates the Binding between Human Papillomavirus 16 L2 and**
886 **Sorting Nexin 27 and Modulates Virion Trafficking**. *J Virol* 2015, **89**:10145–
887 10155.

888 35. Bergant Marušič M, Ozbun MA, Campos SK, Myers MP, Banks L: **Human**
889 **papillomavirus L2 facilitates viral escape from late endosomes via sorting**
890 **nexin 17**. *Traffic* 2012, **13**:455–467.

891 36. Lipovsky A, Popa A, Pimienta G, Wyler M, Bhan A, Kuruvilla L, Guie M-A,
892 Poffenberger AC, Nelson CDS, Atwood WJ, et al.: **Genome-wide siRNA screen**
893 **identifies the retromer as a cellular entry factor for human papillomavirus**.
894 *Proc Natl Acad Sci U S A* 2013, **110**:7452–7457.

895 37. Popa A, Zhang W, Harrison MS, Goodner K, Kazakov T, Goodwin EC, Lipovsky
896 A, Burd CG, DiMaio D: **Direct binding of retromer to human papillomavirus type**

897 **16 minor capsid protein L2 mediates endosome exit during viral infection**.
898 *PLoS Pathog* 2015, **11**:e1004699.

899 38. Day PM, Thompson CD, Schowalter RM, Lowy DR, Schiller JT: **Identification of**
900 **a role for the trans-Golgi network in human papillomavirus 16 pseudovirus**
901 **infection**. *J Virol* 2013, **87**:3862–3870.

902 39. DiGiuseppe S, Luszczek W, Keiffer TR, Bienkowska-Haba M, Guion LGM, Sapp
903 MJ: **Incoming human papillomavirus type 16 genome resides in a vesicular**
904 **compartment throughout mitosis**. *Proc Natl Acad Sci U S A* 2016, **113**:6289–
905 6294.

906 40. Calton CM, Bronnimann MP, Manson AR, Li S, Chapman JA, Suarez-Berumen
907 M, Williamson TR, Molugu SK, Bernal RA, Campos SK: **Translocation of the**
908 **papillomavirus L2/vDNA complex across the limiting membrane requires the**
909 **onset of mitosis**. *PLoS Pathog* 2017, **13**:e1006200.

910 41. Aydin I, Villalonga-Planells R, Greune L, Bronnimann MP, Calton CM, Becker M,
911 Lai K-Y, Campos SK, Schmidt MA, Schelhaas M: **A central region in the minor**
912 **capsid protein of papillomaviruses facilitates viral genome tethering and**
913 **membrane penetration for mitotic nuclear entry**. *PLoS Pathog* 2017,
914 **13**:e1006308.

915 42. Day PM, Baker CC, Lowy DR, Schiller JT: **Establishment of papillomavirus**
916 **infection is enhanced by promyelocytic leukemia protein (PML) expression**.
917 *Proc Natl Acad Sci U S A* 2004, **101**:14252–14257.

918 43. Guion L, Bienkowska-Haba M, DiGiuseppe S, Florin L, Sapp M: **PML nuclear**
919 **body-residing proteins sequentially associate with HPV genome after**
920 **infectious nuclear delivery**. *PLoS Pathog* 2019, **15**:e1007590.

921 44. Schweiger L, Lelieveld-Fast LA, Mikuličić S, Strunk J, Freitag K, Tenzer S,
922 Clement AM, Florin L: **HPV16 Induces Formation of Virus-p62-PML Hybrid**
923 **Bodies to Enable Infection**. *Viruses* 2022, **14**:1478.

924 45. Longworth MS, Laimins LA: **Pathogenesis of human papillomaviruses in**
925 **differentiating epithelia**. *Microbiol Mol Biol Rev* 2004, **68**:362–372.

926 46. McBride AA: **Human papillomaviruses: diversity, infection and host**
927 **interactions**. *Nat Rev Microbiol* 2022, **20**:95–108.

928 47. van Weering JRT, Verkade P, Cullen PJ: **SNX-BAR proteins in**
929 **phosphoinositide-mediated, tubular-based endosomal sorting**. *Semin Cell Dev*
930 *Biol* 2010, **21**:371–380.

931 48. Da Graça J, Morel E: **Canonical and Non-Canonical Roles of SNX1 and SNX2**
932 **in Endosomal Membrane Dynamics**. *Contact (Thousand Oaks)* 2023,
933 **6**:25152564231217867.

934 49. van Weering JRT, Sessions RB, Traer CJ, Kloer DP, Bhatia VK, Stamou D,
935 Carlsson SR, Hurley JH, Cullen PJ: **Molecular basis for SNX-BAR-mediated**
936 **assembly of distinct endosomal sorting tubules**. *EMBO J* 2012, **31**:4466–4480.

937 50. Carlton J, Bujny M, Peter BJ, Oorschot VMJ, Rutherford A, Mellor H,
938 Klumperman J, McMahon HT, Cullen PJ: **Sorting nexin-1 mediates tubular**
939 **endosome-to-TGN transport through coincidence sensing of high- curvature**
940 **membranes and 3-phosphoinositides**. *Curr Biol* 2004, **14**:1791–1800.

941 51. Kurten RC, Cadena DL, Gill GN: **Enhanced degradation of EGF receptors by**
942 **a sorting nexin, SNX1**. *Science* 1996, **272**:1008–1010.

943 52. Rojas R, Kametaka S, Haft CR, Bonifacino JS: **Interchangeable but essential**
944 **functions of SNX1 and SNX2 in the association of retromer with endosomes**
945 **and the trafficking of mannose 6-phosphate receptors**. *Mol Cell Biol* 2007,
946 **27**:1112–1124.

947 53. Simonetti B, Daly JL, Cullen PJ: **Out of the ESCPE room: Emerging roles of**
948 **endosomal SNX-BARs in receptor transport and host–pathogen interaction**.
949 *Traffic* 2023, **24**:234–250.

950 54. Simonetti B, Danson CM, Heesom KJ, Cullen PJ: **Sequence-dependent cargo**
951 **recognition by SNX-BARs mediates retromer-independent transport of CI-**
952 **MPR**. *J Cell Biol* 2017, **216**:3695–3712.

953 55. Kvainickas A, Jimenez-Orgaz A, Nägele H, Hu Z, Dengjel J, Steinberg F: **Cargo-**
954 **selective SNX-BAR proteins mediate retromer trimer independent retrograde**
955 **transport**. *Journal of Cell Biology* 2017, **216**:3677–3693.

956 56. Lopez-Robles C, Scaramuzza S, Astorga-Simon EN, Ishida M, Williamson CD,
957 Baños-Mateos S, Gil-Carton D, Romero-Durana M, Vidaurrazaga A, Fernandez-
958 Recio J, et al.: **Architecture of the ESCPE-1 membrane coat**. *Nat Struct Mol Biol*
959 2023, **30**:958–969.

960 57. Atwell B, Chen C-Y, Christofferson M, Montfort WR, Schroeder J: **Sorting nexin-**
961 **dependent therapeutic targeting of oncogenic epidermal growth factor**
962 **receptor**. *Cancer Gene Ther* 2022, doi:10.1038/s41417-022-00541-7.

963 58. Ho A, Schwarze SR, Mermelstein SJ, Waksman G, Dowdy SF: **Synthetic**
964 **Protein Transduction Domains: Enhanced Transduction Potential in Vitro and**
965 **in Vivo1**. *Cancer Research* 2001, **61**:474–477.

966 59. Reichelt J, Haase I: **Establishment of spontaneously immortalized**
967 **keratinocyte lines from wild-type and mutant mice**. *Methods Mol Biol* 2010,
968 **585**:59–69.

969 60. Zhang W, Kazakov T, Popa A, DiMaio D: **Vesicular trafficking of incoming**
970 **human papillomavirus 16 to the Golgi apparatus and endoplasmic reticulum**
971 **requires γ-secretase activity**. *mBio* 2014, **5**:e01777-01714.

972 61. Cardone G, Moyer AL, Cheng N, Thompson CD, Dvoretzky I, Lowy DR, Schiller
973 JT, Steven AC, Buck CB, Trus BL: **Maturation of the human papillomavirus 16**
974 **capsid**. *mBio* 2014, **5**:e01104-01114.

975 62. Schneider CA, Rasband WS, Eliceiri KW: **NIH Image to ImageJ: 25 years of**
976 **image analysis**. *Nat Methods* 2012, **9**:671–675.

977 63. **Measuring cell fluorescence using ImageJ — The Open Lab Book v1.0**.
978 [date unknown],

979 64. Schrödinger, LLC: **The PyMOL Molecular Graphics System, Version 1.8**.
980 2015,

981 65. Thompson JD, Higgins DG, Gibson TJ: **CLUSTAL W: improving the sensitivity**
982 **of progressive multiple sequence alignment through sequence weighting,**
983 **position-specific gap penalties and weight matrix choice.** *Nucleic Acids Res*
984 1994, **22**:4673–4680.

985 66. Szklarczyk D, Kirsch R, Koutrouli M, Nastou K, Mehryary F, Hachilif R, Gable AL,
986 Fang T, Doncheva NT, Pyysalo S, et al.: **The STRING database in 2023: protein-**
987 **protein association networks and functional enrichment analyses for any**
988 **sequenced genome of interest**. *Nucleic Acids Res* 2023, **51**:D638–D646.

989 67. **STRING: functional protein association networks**. [date unknown],

990 68. Pyeon D, Pearce SM, Lank SM, Ahlquist P, Lambert PF: **Establishment of**
991 **human papillomavirus infection requires cell cycle progression**. *PLoS Pathog*
992 2009, **5**:e1000318.

993 69. Campos SK, Chapman JA, Deymier MJ, Bronnimann MP, Ozbun MA: **Opposing**
994 **effects of bacitracin on human papillomavirus type 16 infection: enhancement**
995 **of binding and entry and inhibition of endosomal penetration**. *J Virol* 2012,
996 **86**:4169–4181.

997 70. Calton CM, Schlegel AM, Chapman JA, Campos SK: **Human papillomavirus**
998 **type 16 does not require cathepsin L or B for infection**. *J Gen Virol* 2013,
999 **94**:1865–1869.

1000 71. Galloway CJ, Dean GE, Marsh M, Rudnick G, Mellman I: **Acidification of**
1001 **macrophage and fibroblast endocytic vesicles in vitro**. *Proc Natl Acad Sci U S A*
1002 1983, **80**:3334–3338.

1003 72. Aydin I, Weber S, Snijder B, Samperio Ventayol P, Kühbacher A, Becker M, Day
1004 PM, Schiller JT, Kann M, Pelkmans L, et al.: **Large scale RNAi reveals the**

1005 **requirement of nuclear envelope breakdown for nuclear import of human**
1006 **papillomaviruses**. *PLoS Pathog* 2014, **10**:e1004162.

1007 73. Barker DF, Campbell AM: **The birA gene of Escherichia coli encodes a biotin**
1008 **holoenzyme synthetase**. *J Mol Biol* 1981, **146**:451–467.

1009 74. Schatz PJ: **Use of peptide libraries to map the substrate specificity of a**
1010 **peptide-modifying enzyme: a 13 residue consensus peptide specifies**
1011 **biotinylation in Escherichia coli**. *Biotechnology (N Y)* 1993, **11**:1138–1143.

1012 75. Campos SK: **Subcellular Trafficking of the Papillomavirus Genome during**
1013 **Initial Infection: The Remarkable Abilities of Minor Capsid Protein L2**. *Viruses*
1014 2017, **9**.

1015 76. Ikegami S, Taguchi T, Ohashi M, Oguro M, Nagano H, Mano Y: **Aphidicolin**
1016 **prevents mitotic cell division by interfering with the activity of DNA**
1017 **polymerase-alpha**. *Nature* 1978, **275**:458–460.

1018 77. Li S, Bronnimann MP, Williams SJ, Campos SK: **Glutathione contributes to**
1019 **efficient post-Golgi trafficking of incoming HPV16 genome**. *PLoS One* 2019,
1020 **14**:e0225496.

1021 78. Li C: **Specific cell cycle synchronization with butyrate and cell cycle**
1022 **analysis**. *Methods Mol Biol* 2011, **761**:125–136.

1023 79. Zhang P, Monteiro da Silva G, Deatherage C, Burd C, DiMaio D: **Cell-**
1024 **Penetrating Peptide Mediates Intracellular Membrane Passage of Human**
1025 **Papillomavirus L2 Protein to Trigger Retrograde Trafficking**. *Cell* 2018,
1026 **174**:1465-1476.e13.

1027 80. Nishimura Y, Itoh K: **Involvement of SNX1 in regulating EGFR endocytosis in**
1028 **a gefitinib-resistant NSCLC cell lines**. *Cancer Drug Resist* 2019, **2**:539–549.

1029 81. Yang Z, Feng Z, Li Z, Teasdale RD: **Multifaceted Roles of Retromer in EGFR**
1030 **Trafficking and Signaling Activation**. *Cells* 2022, **11**:3358.

1031 82. Day TF, Kallakury BVS, Ross JS, Voronel O, Vaidya S, Sheehan CE, Kasid UN:
1032 **Dual Targeting of EGFR and IGF1R in the TNFAIP8 Knockdown Non-Small Cell**
1033 **Lung Cancer Cells**. *Mol Cancer Res* 2019, **17**:1207–1219.

1034 83. Brinkert P, Krebs L, Ventayol PS, Greune L, Bannach C, Bucher D, Kollasser J,
1035 Dersch P, Boulant S, Stradal TEB, et al.: **Endocytic vacuole formation by WASH-**
1036 **mediated endocytosis**. *bioRxiv* 2021, doi:10.1101/2021.06.18.448076.

1037 84. Yong X, Zhao L, Deng W, Sun H, Zhou X, Mao L, Hu W, Shen X, Sun Q,
1038 Billadeau DD, et al.: **Mechanism of cargo recognition by retromer-linked SNX-**
1039 **BAR proteins**. *PLoS Biol* 2020, **18**:e3000631.

1040 85. Gokool S, Tattersall D, Seaman MNJ: **EHD1 Interacts with Retromer to**
1041 **Stabilize SNX1 Tubules and Facilitate Endosome-to-Golgi Retrieval**. *Traffic*
1042 2007, **8**:1873–1886.

1043 86. Xie J, Zhang P, Crite M, Lindsay CV, DiMaio D: **Retromer stabilizes transient**
1044 **membrane insertion of L2 capsid protein during retrograde entry of human**
1045 **papillomavirus**. *Sci Adv* 2021, **7**:eabh4276.

1046 87. Siddiqa A, Massimi P, Pim D, Broniarczyk J, Banks L: **Human Papillomavirus**
1047 **16 Infection Induces VAP-Dependent Endosomal Tubulation**. *J Virol* 2018, **92**.

1048 88. Siddiqa A, Massimi P, Pim D, Banks L: **Diverse Papillomavirus Types Induce**
1049 **Endosomal Tubulation**. *Front Cell Infect Microbiol* 2019, **9**:175.

1050 89. Da Graça J, Charles J, Djebar M, Alvarez-Valadez K, Botti J, Morel E: **A SNX1-**
1051 **SNX2-VAPB partnership regulates endosomal membrane rewiring in response**
1052 **to nutritional stress**. *Life Sci Alliance* 2023, **6**:e202201652.

1053 90. Pujals S, Miyamae H, Afonin S, Murayama T, Hirose H, Nakase I, Taniuchi K,
1054 Umeda M, Sakamoto K, Ulrich AS, et al.: **Curvature engineering: positive**
1055 **membrane curvature induced by epsin N-terminal peptide boosts**
1056 **internalization of octaarginine**. *ACS Chem Biol* 2013, **8**:1894–1899.

1057 91. Zakany F, Mándity IM, Varga Z, Panyi G, Nagy P, Kovacs T: **Effect of the Lipid**
1058 **Landscape on the Efficacy of Cell-Penetrating Peptides**. *Cells* 2023, **12**:1700.

1059

1060

1061

1062

1063

1064

1065

1066

1067

1068

1069

1070 **Figure 1**

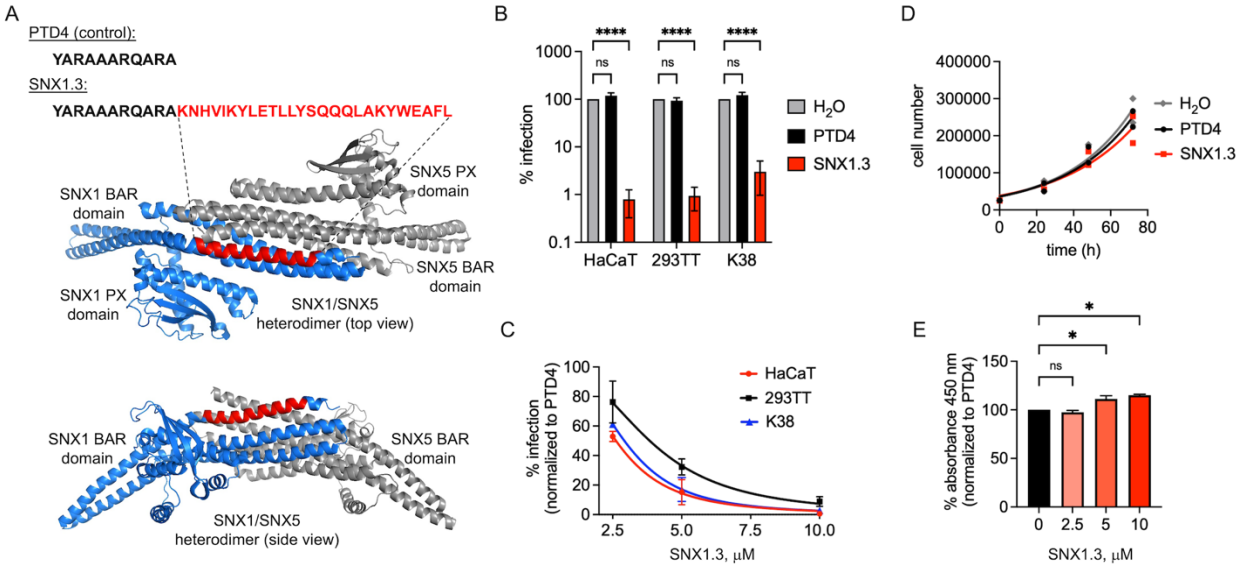

1071

1072

1073

1074

1075

1076

1077

1078

1079

1080

1081

1082

1083

1084

1085

1086 **Figure 2**

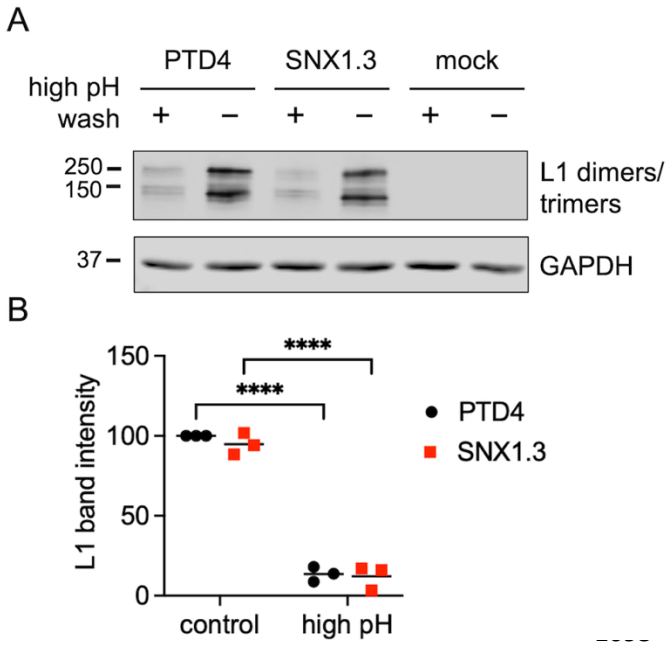

1096

1097

1098

1099

1100

1101

1102

1103

1104

1105

1106

1107

1108

1109 **Figure 3**

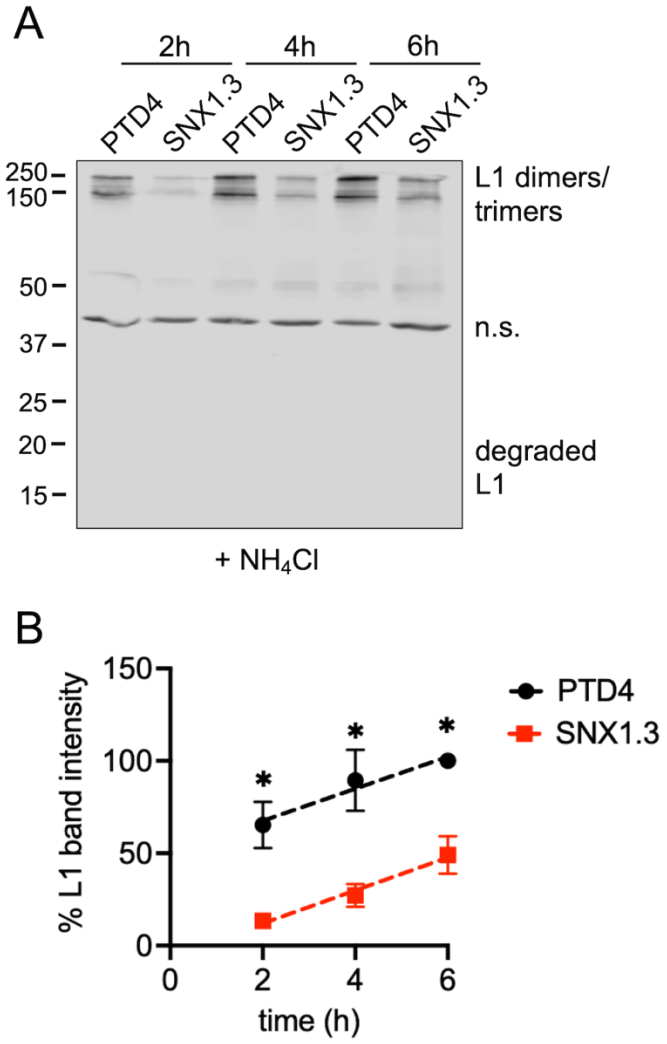

1124

1125

1126

1127

1128

1129

1130

1131 **Figure 4**

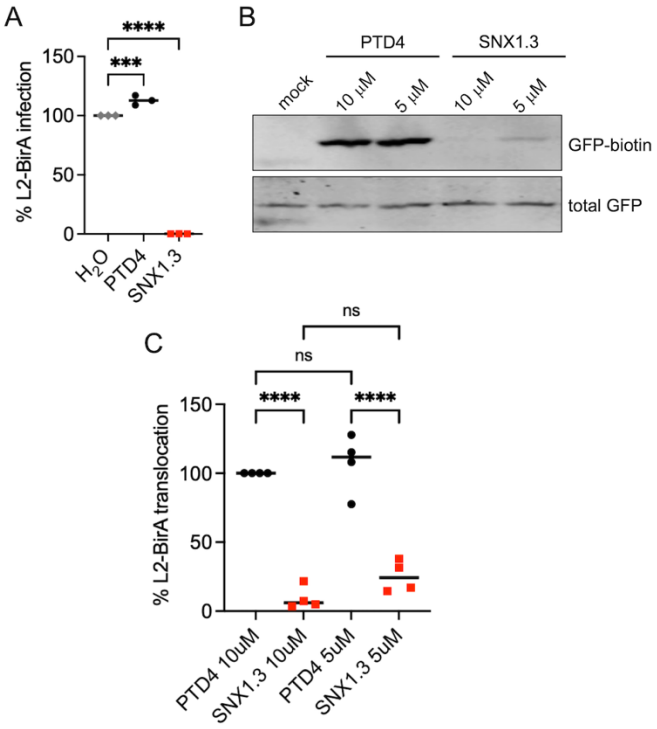

1132

1133

1134

1135

1136

1137

1138

1139

1140

1141

1142

1143

1144 **Figure 5**

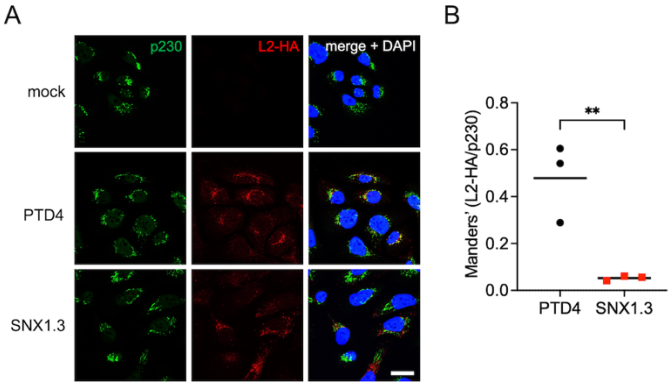

1145

1146

1147

1148

1149

1150

1151

1152

1153

1154

1155

1156

1157

1158

1159

1160

1161

1162 **Figure 6**

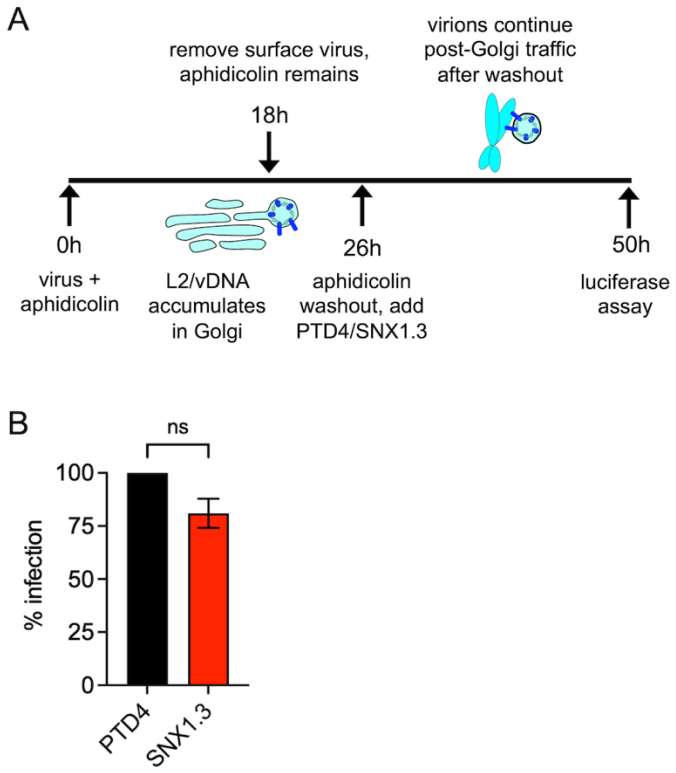

1163

1164

1165

1166

1167

1168

1169

1170

1171

1172

1173

1174

1175 **Figure 7**

1176

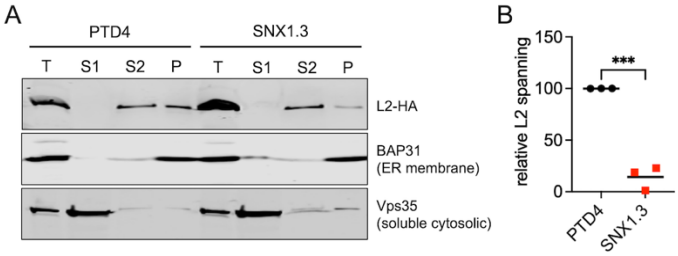

1177

1178

1179

1180

1181

1182

1183

1184

1185

1186

1187

1188

1189

1190

1191

1192

1193

1194

1195 **Figure 8**

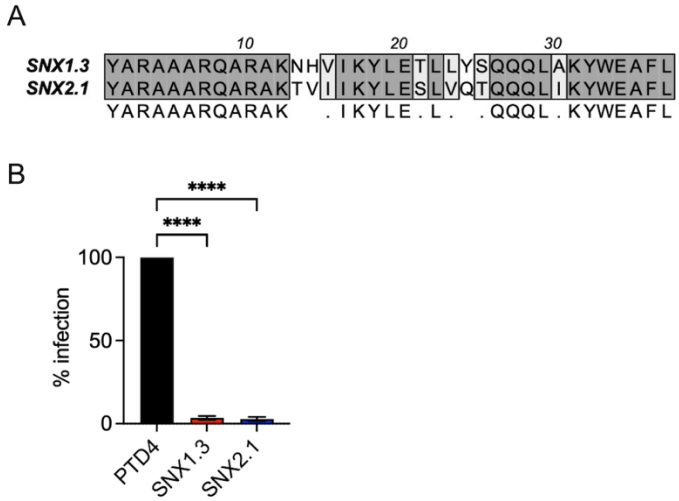

Supplemental Figure 1

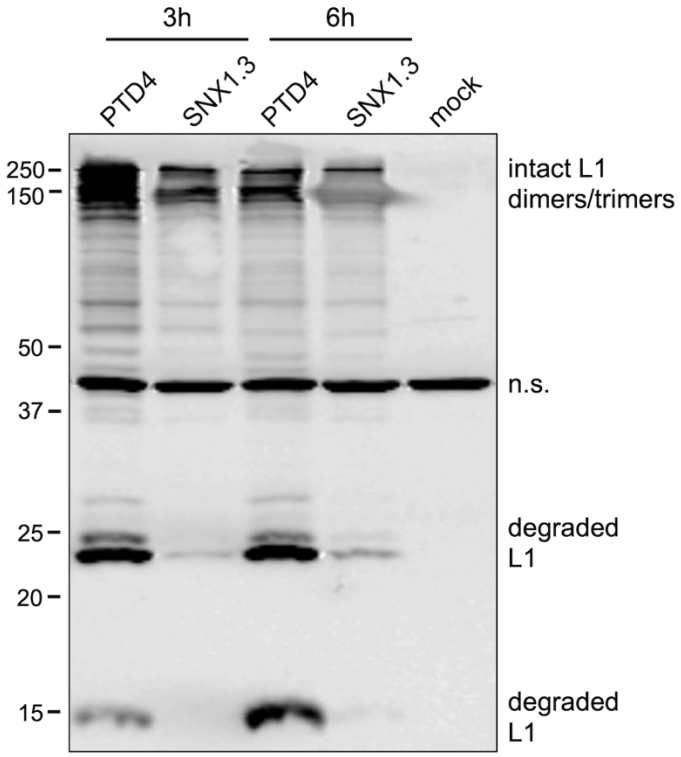

Supplemental Figure 2

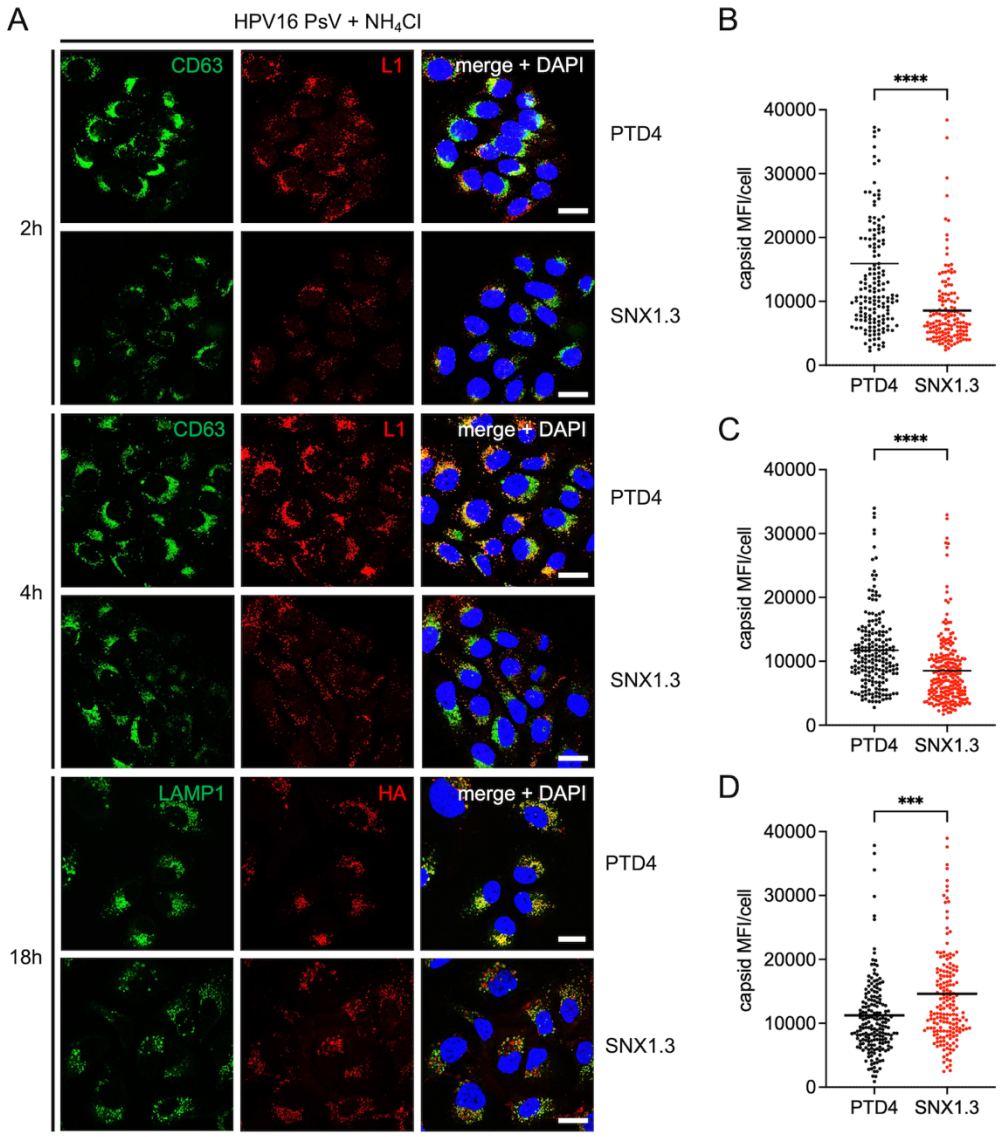

1225

1226

1227

1228

1229

1230

1231

1232 **Supplemental Figure 3**

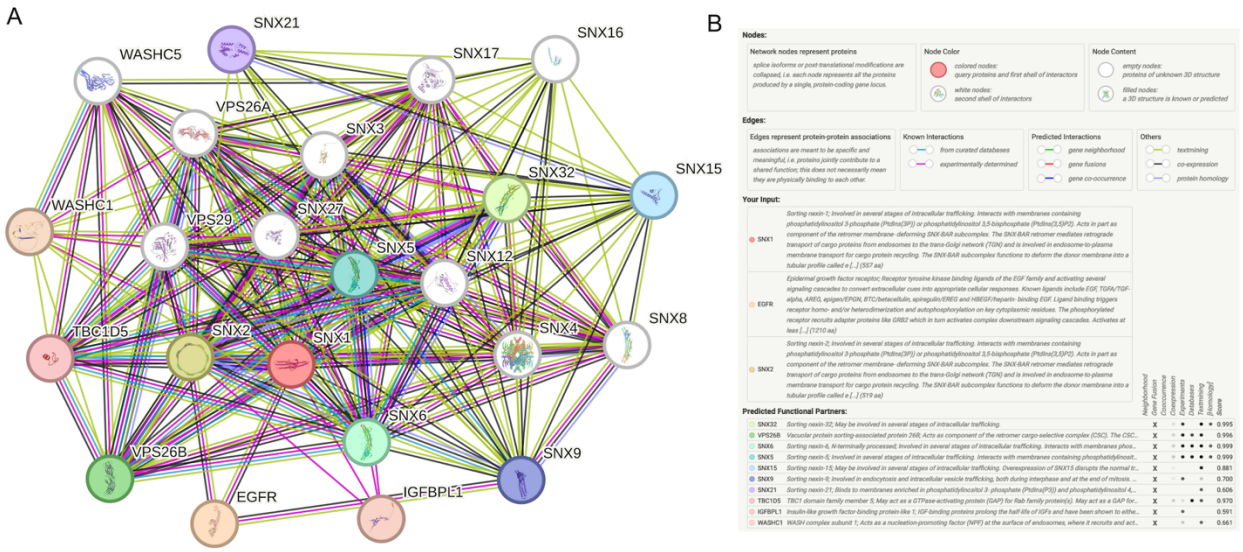
A
SNX21
WASHC5
SNX17
SNX16
VPS26A
SNX3
SNX32
SNX15
WASHC1
VPS29
SNX27
SNX5
SNX12
SNX8
TBC1D5
SNX2
SNX1
SNX4
SNX6
VPS26B
SNX9
EGFR
IGFBPL1
B
Nodes:
Network nodes represent proteins
splice isoforms or post-translational modifications are collapsed, i.e. each node represents all the proteins produced by a single, protein-coding gene locus.
Node Color
colored nodes: query proteins and first shell of interactors
white nodes: second shell of interactors
Node Content
empty nodes: proteins of unknown 3D structure
filled nodes: a 3D structure is known or predicted
Edges:
Edges represent protein-protein associations
associations are meant to be specific and meaningful, i.e. proteins jointly contribute to a shared function; this does not necessarily mean they are physically binding to each other.
Known Interactions
from curated databases
experimentally determined
Predicted Interactions
gene neighborhood
gene fusions
gene co-occurrence
Others
textmining
co-expression
protein homology
Your Input:
SNX1 Sorting nexin-1; Involved in several stages of intracellular trafficking. Interacts with membranes containing phosphatidylinositol 3-phosphate (PtdIns(3P)) or phosphatidylinositol 3,5-bisphosphate (PtdIns(3,5)P2). Acts in part as component of the retromer membrane- deforming SNX-BAR subcomplex. The SNX-BAR retromer mediates retrograde transport of cargo proteins from endosomes to the trans-Golgi network (TGN) and is involved in endosome-to-plasma membrane transport for cargo protein recycling. The SNX-BAR subcomplex functions to deform the donor membrane into a tubular profile called e [...] (557 aa)
EGFR Epidermal growth factor receptor; Receptor tyrosine kinase binding ligands of the EGF family and activating several signaling cascades to convert extracellular cues into appropriate cellular responses. Known ligands include EGF, TGFA/TGF-alpha, AREG, epigen/EPGN, BTC/betacellulin, epiregulin/EREG and HBEGF/heparin- binding EGF. Ligand binding triggers receptor homo- and/or heterodimerization and autophosphorylation on key cytoplasmic residues. The phosphorylated receptor recruits adapter proteins like GRB2 which in turn activates complex downstream signaling cascades. Activates at least [...] (1210 aa)
SNX2 Sorting nexin-2; Involved in several stages of intracellular trafficking. Interacts with membranes containing phosphatidylinositol 3-phosphate (PtdIns(3P)) or phosphatidylinositol 3,5-bisphosphate (PtdIns(3,5)P2). Acts in part as component of the retromer membrane- deforming SNX-BAR subcomplex. The SNX-BAR retromer mediates retrograde transport of cargo proteins from endosomes to the trans-Golgi network (TGN) and is involved in endosome-to-plasma membrane transport for cargo protein recycling. The SNX-BAR subcomplex functions to deform the donor membrane into a tubular profile called e [...] (519 aa)
Neighborhood
Gene Fusion
Co-occurrence
Co-expression
Experiments
Database
Textmining
Homology
Score
Predicted Functional Partners:
SNX32 Sorting nexin-32; May be involved in several stages of intracellular trafficking. X 0.995
VPS26B Vacuolar protein sorting-associated protein 26B; Acts as component of the retromer cargo-selective complex (CSC). The CSC... X 0.996
SNX6 Sorting nexin-6, N-terminally processed; Involved in several stages of intracellular trafficking. Interacts with membranes phosp... X 0.999
SNX5 Sorting nexin-5; Involved in several stages of intracellular trafficking. Interacts with membranes containing phosphatidylinosit... X 0.999
SNX15 Sorting nexin-15; May be involved in several stages of intracellular trafficking. Overexpression of SNX15 disrupts the normal tr... X 0.881
SNX9 Sorting nexin-9; Involved in endocytosis and intracellular vesicle trafficking, both during interphase and at the end of mitosis. ... X 0.700
SNX21 Sorting nexin-21; Binds to membranes enriched in phosphatidylinositol 3- phosphate (PtdIns(P3)) and phosphatidylinositol 4,... X 0.606
TBC1D5 TBC1 domain family member 5; May act as a GTPase-activating protein (GAP) for Rab family protein(s). May act as a GAP for... X 0.970
IGFBPL1 Insulin-like growth factor-binding protein-like 1; IGF-binding proteins prolong the half-life of IGFs and have been shown to eithe... X 0.591
WASHC1 WASH complex subunit 1; Acts as a nucleation-promoting factor (NPF) at the surface of endosomes, where it recruits and act... X 0.661

1233

1234